Tang *et al. Cardiovascular Diabetology* (2025) 24:121
https://doi.org/10.1186/s12933-025-02638-3

Cardiovascular Diabetology

RESEARCH Open Access

GPR30-driven fatty acid oxidation targeted by ginsenoside Rd maintains mitochondrial redox homeostasis to restore vascular barrier in diabetic retinopathy

Kai Tang[1], Congcong Huang[1], Zhengjie Huang[1], Zhen Wang[1*] and Ninghua Tan[1*]

Abstract

Blood-retinal barrier (BRB) breakdown, a pivotal contributor to multiple retinal vascular diseases, manifests as a progressive increase in vascular permeability induced by various pathological stimuli. The functional plasticity of retinal endothelial cells can be intricately shaped by metabolic alteration. However, little is known about the mechanisms through which endothelial metabolic disorders trigger the dissolution of inter-vascular junctions and the selective approaches to targeting metabolic homeostasis. Herein, we identify AMPK-associated fatty acid oxidation (FAO) inhibition as a critical driver of vascular barrier dysfunction via exacerbating redox imbalance. Pharmacological facilitation of FAO by ginsenoside Rd (Rd) suppresses BRB collapse and other secondary retinal damage in diabetic retinopathy (DR). Mechanistically, Rd targets GPR30 to phosphorylate AMPK via the PKA-LKB1-AMPK kinase cascade. The AMPK activation induced by Rd revitalizes hyperglycemia-compromised FAO, and then sustains mitochondrial NADPH regeneration by emphasis on IDH2 at various levels, including substrate supply, transcription, and post-translational modifications. Therefore, Rd alleviates the disruption of BRB integrity driven by mitochondrial oxidative stress, with the vasculoprotection of Rd diminished by GPR30 knockdown and pharmacological attenuation of AMPK. These findings collectively reveal the previously-unanticipated role of endothelial FAO in heightened retinal vascular leakage, and highlight the potential translational application of GPR30 agonism with Rd to mitigate barrier dysfunction, providing a metabolic regulatory therapeutic strategy for DR.

Keywords Diabetic retinopathy, Ginsenoside Rd, Blood-retinal barrier, Fatty acid oxidation, GPR30, Mitochondrial oxidative stress

*Correspondence:
Zhen Wang
drwang@cpu.edu.cn
Ninghua Tan
nhtan@cpu.edu.cn

Full list of author information is available at the end of the article

Graphical Abstract

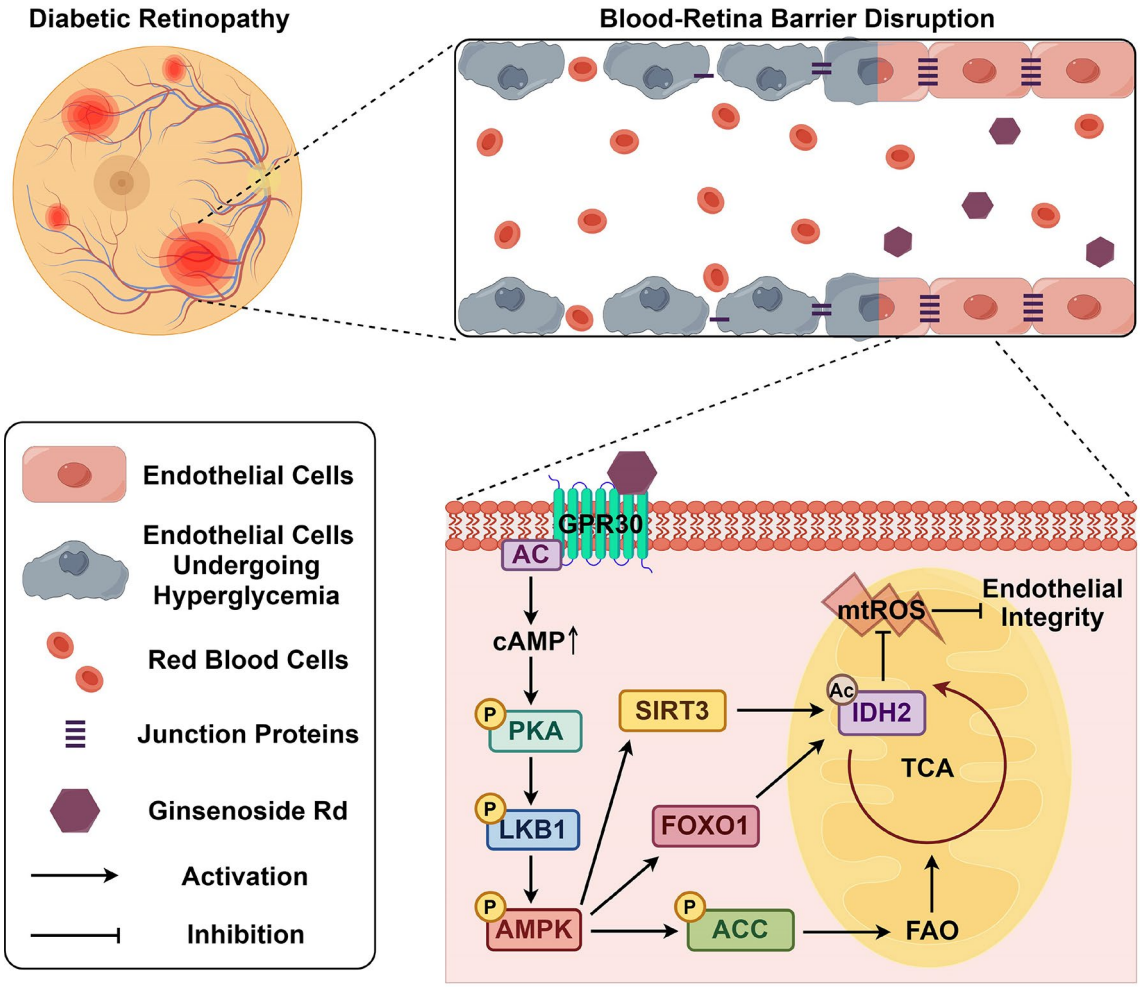

Introduction

Diabetic retinopathy (DR) emerges as a prevalent and serious diabetic microvascular complication, affecting approximately one-third of individuals with diabetes mellitus [1–2]. As the prevalence of diabetes mellitus continues to rise, DR has gradually become the leading cause of blindness in adults [3]. Although the clinical manifestations of DR are diverse and intricate, the progressive vascular barrier dysfunction and the subsequent compromise of blood-retinal barrier (BRB) integrity exhibit a close connection with all known clinical symptoms of DR [4–5]. The current approach to treating early DR primarily relies on strict metabolic control of diabetes until the disease progresses to the advanced stage, necessitating vitreous injections of vascular endothelial growth factor (VEGF) antibodies and other invasive and destructive therapies [4, 6]. Characterized by its insidious onset, poor prognosis and limited treatment options, initial prevention of lesions in DR carries profound clinical and societal significance, before visual symptoms become irreversible.

Endothelial cell (EC) metabolism plays a critical role in determining the vascular function [7–8]. Nevertheless, the extent to which abnormal retinal endothelial metabolism contributes to these phenotypic changes in DR remains largely unexplored. Clinical studies have frequently revealed dysregulated lipid metabolism resulting from hyperglycemia in cases of DR [9]. Consequently, hyperlipemia has been proposed as a potential risk factor for DR, and the use of fibrates has shown protective effects against retinal vascular damage [10]. Most findings around retinal vascular metabolism have centered on enhanced vessel sprouting through endothelial glycolysis [11]. Further investigation is warranted to understand the specific mechanisms by which endothelial lipid metabolism maintains phenotypic homeostasis of DR, in consideration of the powerful vaso-regulatory activity of lipid metabolism in other diabetic complications [12].

AMP-activated protein kinase (AMPK) serves as a sensitive sensor of cellular energy levels, capable of being activated by AMP accumulation as well as various upstream kinases [13]. In instances of depleted energy, the phosphorylated AMPK re-establishes ATP balance and adapts to nutrient availability by inhibiting anabolism and facilitating catabolism. The hyperglycemia-induced inhibition of AMPK fosters intraocular inflammation, pericyte apoptosis, and reduced retinal blood flow in diverse models of DR [14]. Moreover, numerous clinical drugs and natural products improve neurovascular injury of DR in an AMPK-dependent manner [14–15]. GPR30, a member of the estrogen receptor family, affects vascular function and cell metabolism, but has not been investigated in retinal diseases [16–17]. Based on the preceding discoveries, it is plausible to hypothesize that AMPK and GPR30 may be involved in regulating the retinal endothelial dysfunction caused by metabolic disturbances in diabetic conditions.

Ginsenoside Rd (Rd) is a natural tetracyclic triterpenoid, served as the principal medicinal constituent in *Panax notoginseng* (Burk.) F. H. Chen [18]. *Notoginseng* Radix et Rhizoma (Sanqi) and its compound preparation are commonly prescribed in clinical settings for the treatment of DR [19]. Previous pharmacological investigations have primarily concentrated on the neuroprotective effects of Rd in neurological and cerebrovascular disorders [20]. Our prior research has demonstrated that Rd facilitates the interaction between AMPK and SIRT1 in ECs by increasing the levels of NAD^+/NADH and deacetylating LKB1. The emphasis on AMPK/SIRT1 interaction by Rd beneficially reduces ROS production, reverses endothelial mitochondrial intrinsic apoptosis, and ultimately ameliorates diabetes-driven retinal vascular damage [21]. The specific upstream mechanisms by which Rd activates AMPK and the target molecules for treating DR are still not fully understood. Thereby, this study aims to explore the significance of AMPK-related lipid metabolism derangements in endothelial dysfunction induced by hyperglycemia. Additionally, a metabolic perspective is employed to further elucidate the vasculoprotective mechanism of Rd in DR and identify the potential therapeutic targets.

Materials and methods

Animals

C57BL/6 male mice (No: SCXK [Su] 2018-0006), aged 6–8 weeks, were procured from Shanghai Sippr-BK Laboratory Animal Co. Ltd. (Shanghai, China). Animals were housed and provided with standard laboratory conditions, including a 12h light/dark cycle, *ad libitum* access to drinking water, and standard laboratory chow. All animal studies were conducted in accordance with the guidelines set by the National Institutes of Health, and reviewed and approved by the Institutional Animal Care and Use Committee of China Pharmaceutical University and the Institutional Ethics Committee of China Pharmaceutical University (approval number: 2023-08-017). A deliberate endeavor was undertaken to mitigate the harm caused to animals and reduce the quantity of animals utilized. The animal studies were methodically designed to ensure the formation of groups of equal size through the implementation of randomized and blinded analysis techniques.

For knockdown, recombinant AAV8 vectors carrying shRNA targeting mouse GPR30 (GenePharma, Shanghai, China) were used. In brief, C57BL/6 male mice were subjected to intravitreal injection of 5 μl AAV8-sh*GPR30* (virus titer > 10^{12} viral genomes/mL) one week prior to STZ administration. Control mice were injected with an equal volume of AAV8-control suspension. The efficiency of AAV transduction in vivo was assessed through Western blot analysis.

STZ-induced diabetic model

The DR model was established in C57BL/6 mice via intraperitoneal injection of STZ. The fasted mice received 55 mg/kg of STZ via intraperitoneal injection for five consecutive days. Control animals were administered with an equivalent volume of sterile citrate buffer. Fasting blood glucose levels were measured using a glucometer (Roche, Mannheim, Germany) one week after the final injection. Mice exhibiting blood glucose levels above 16.7 mM, along with other characteristic symptoms of diabetes, were considered to have successfully undergone modeling.

In the pharmacodynamic studies, the mice were separated into five groups: normal control (A1), DR model (B1), 0.5% Rd eye drops (C1), 1% Rd eye drops (D1), and 100 mg/kg CaD (F1). Mice in groups A1 and B1 were given an equal volume of vehicle eye drops. Groups C1 and D1 were subjected to daily administration of 5 μl of 0.5 or 1% (*w/v*) Rd eye drops. 100 mg/kg CaD was administered daily to mice in group F1 by oral administration.

In mechanistic studies for lipid metabolism, the mice were separated into five groups: normal control (A2), DR model (B2), 1% Rd eye drops (C2), 1% Rd eye drops + Eto (D2), and Mito-TEMPO (E2). Groups C2 and D2 were administered with 5 μl 1% (*w/v*) Rd eye drops every day. 1 μl of Eto (200 μM) or Mito-TEMPO (200 μM) was injected into vitreous of mice in group D2 or E2 once a week.

In mechanistic studies for GPR30, the mice were separated into six groups: normal control (A3), DR model (B3), 1% Rd eye drops (C3), 1% Rd eye drops + AAV8-sh*GPR30* (D3), 1% Rd eye drops + AAV8-NC (E3), and 100 μM G1 (F3). Groups C3, D3 and E3 were administered with 5 μl 1% (*w/v*) Rd eye drops every day. 1 μl of

G1 (100 μM) was injected into vitreous of mice in group F3 once a week.

Following three months of uninterrupted administration, the retinal tissue samples were collected for subsequent analysis. The preparation of eye drops and other drug dosages were conducted according to the previous report [21].

Evans blue dye leakage

Evans blue dye leakage assay was carried out as detailed previously [21]. Briefly, the left heart ventricle of mice was cannulated and perfused with PBS, after injection of 50 mg/kg Evans blue (Sigma) and full circulation. After fixation, the retinas were removed from eye cups. The dye concentration in the retina was measured with a multi-mode microplate reader (Biotek Epoch, Winooski, VT, USA), and the representative pictures were taken with a fluorescence microscope (Leica DMi8, Wetzlar, Heessen, Germany).

Histological analysis

Retinal trypsin digestion assay and Hematoxylin & Eosin (HE) staining assay were performed as previously reported [21]. The retinas were fixed in 10% neutral formalin over 24 h. For retinal trypsin digestion, the retinas were incubated in trypsin until the medium became cloudy and the peeled vessel networks were stained with PAS-hematoxylin. For HE staining, the paraffin sections of eye tissues were dewaxed and dehydrated, and then stained with Hematoxylin and Eosin. Representative pictures were obtained by an optical microscope (Leica DMi8, Wetzlar, Heessen, Germany).

Western blot

The mice retina and cells were lysed in RIPA buffer with PMSF to extract total protein. The cytosolic and nuclear proteins were isolated as described in the nucleoprotein extraction kit (Beyotime Biotechnology, Nanjing, Jiangsu, China). The protein estimation was conducted using BCA protein assay. Equal amounts of the collective proteins were separated by SDS-PAGE gels and transferred onto PVDF membranes. After blocked with 5% BSA, the membranes were incubated with specific primary antibodies overnight at 4 °C. Following removal of unbound antibody, the membranes were probed with HRP-conjugated secondary antibodies. The protein imaging was performed on Tanon 5200 multi chemiluminescent substrate system (Tanon, Shanghai, China) and analyzed by Image-Pro Plus 6.0 (IPP 6.0) software.

RNA isolation and quantitative real-time PCR

The total RNA from cells was extracted using Trizol reagent (Takara, Otsu, Japan) according to the manufacturer's instructions. cDNA transcribed from the templet RNA was synthesized using HiScript II Q RT SuperMix (Vazyme, Nanjing, Jiangsu, China). Real-time qPCR was performed using Ace qPCR SYBR Green Master Mix (Vazyme, Nanjing, Jiangsu, China) with a StepOne Real-Time PCR System (Applied Biosystems). The primer sequences used in the study were shown in Supplementary file 1: Table S1. The mRNA relative expression of target genes was normalized to *GAPDH* and analyzed using the $2^{-\Delta\Delta Ct}$ method.

FITC-dextran leakage assay

Endothelial cell permeability was monitored via the leakage of FITC-dextran. Primary rat retinal vascular endothelial cells (RVECs) were grown to confluence on transwell inserts (0.4 μm; Millipore). After treatment, 1 mg/ml FITC-dextran (70 kDa) was added into the upper wells of the transwell inserts. Following 4 h incubation, the fluorescence intensity of FITC-dextran in the medium of the lower wells was measured by multi-mode microplate reader (Biotek Epoch). The fluorescence intensity was converted into concentration through the standard curve.

Transendothelial electrical resistance assay

RVECs were cultured on transwell inserts (0.4 μm; Millipore), and received different treatments. Transendothelial electrical resistance (TER) was determined by Millicell-ERS voltohmmeter together with an electrode (Millipore, USA). The TER value was expressed as the common unit ($\Omega \cdot cm^2$) after background-correction by subtraction of the value of a blank cell-free insert.

Detection of oxygen consumption rate

FAO was measured using XF palmitate oxidation stress test kit (Seahorse Bioscience, MA, USA) according to the manufacturer recommended protocols. Briefly, RVECs (8000 per well) were seeded in XF96 cell culture microplates precoated with fibronectin. After starvation in substrate limited medium (500 μM glucose, 1 mM L-glutamine, 0.5 mM L-carnitine and 1% FBS), the cells were replaced with FAO assay medium (111 mM NaCl, 4.7 mM KCl, 1.25 mM $CaCl_2$, 2 mM $MgSO_4$, 1.2 mM NaH_2PO_4, 2.5 mM glucose, 500 μM L-carnitine, and 5 mM HEPES). Immediately before the assay, either BSA or palmitate-BSA FAO substrate was added to the predetermined wells. The oxygen consumption rate (OCR) was continuously measured in real-time following injections of oligomycin (1 μg/ml), FCCP (1 μM), rotenone (0.5 μM), and antimycin A (0.5 μM). The OCR were normalized according to protein concentrations.

Microscale thermophoresis assay

The binding affinity of Rd for GPR30 was determined using microscale thermophoresis assay (MST). HEK293T

cells were transfected with the plasmids encoding EGFP-tagged GPR30 (GenePharma) and the lysate cell supernatant was collected for MST experiments. The samples were loaded in MST standard capillaries and analyzed by NT.115 NanoTemper Monolith Instrument (NanoTemper, Germany).

Statistical analysis

Data were presented as the mean ± standard error of the mean (SEM). All statistical analyses and plots were generated using GraphPad Prism software (San Diego, CA, USA). Statistical variation between two groups by using the two-tailed Student's *t*-test. Multi-group comparisons were evaluated utilizing one-way ANOVA with Tukey's test. p-value < 0.05 was considered statistically significant.

Results

Ginsenoside Rd attenuated diabetes-related endothelial barrier dysfunction in vitro and in vivo

Notoginseng Radix et Rhizoma and its primary components *i.e. Panax notoginseng* saponins (PNS) had been found to strengthen the barrier function of the retinal vessels in DR [19, 22]. In this study, an in vitro model of DR was established in high glucose-induced RVECs. The EC permeability and immunoblot assays were conducted to screen the main ginsenosides in PNS (Fig. 1a and Supplementary file 1: Fig. S1b-c). Subsequently, four saponins (ginsenoside Rg1, Rb1, Rd, and Rc) with superior in vitro activities were topically administered to mice intravitreally injected with VEGF. Among these saponins, ginsenoside Rd efficiently inhibited the acute augmentation of vascular permeability in response to VEGF (Fig. 1b). Accordingly, Rd was selected for the further investigation.

Our previous research demonstrated that Rd exerted anti-apoptotic effects on retinal ECs via preserving redox homeostasis [21]. The involvement of oxidative stress in the BRB impairment and DR had been extensively established [5, 23]. The collapse of BRB was characterized through the FITC-dextran flux across EC monolayer and the transendothelial electrical resistance (TER) analysis in vitro. High glucose exposure elevated the levels of total ROS and superoxide anion in RVECs, which resulted in a disruption of endothelial monolayer integrity and polarity (Fig. 1c-f). The permeability of vascular barrier was mainly controlled by inter-endothelial adherens junctions, tight junctions, and gap junctions [23]. High glucose blunted the expression of proteins associated with adherens junctions (VE-cadherin), tight junctions (ZO-1 and Occludin) and gap junctions (Cx43), thereby impeding the function of BRB (Fig. 1g and Supplementary file 1: Fig. S1d-g). In normal RVECs, the immunostaining for VE-cadherin and ZO-1 appeared as a continuous band at the junctions of retinal EC, whereas high glucose dampened and broke the immunostaining pattern (Fig. 1h and Supplementary file 1: Fig. S1h-i). In high glucose-treated RVECs, Rd attenuated the fluorescence intensities of DCFH and DHE (Fig. 1c-d). The loss of endothelial monolayer integrity and polarity was reversed by Rd in a concentration-dependent manner (Fig. 1e-f). Rd boosted the level of vascular barrier function-related proteins in RVECs (Fig. 1g-h and Supplementary file 1: Fig. S1d-i). Additionally, calcium dobesilate (CaD), a common drug for diabetic microvascular complications, partially restored the aforementioned alterations in endothelial function (Fig. 1c-h and Supplementary file 1: Fig. S1d-i). To further validate the screening findings and elucidate the in vivo efficacy of Rd, a mouse model with STZ-induced hyperglycemia was employed. HE staining highlighted the decreased retinal thickness, disorganized retinal architecture and neuronal cell loss in the DR mice. The above pathological changes were significantly alleviated by Rd in a dose-dependent manner (Fig. 1i and Supplementary file 1: Fig. S1j). Meanwhile, Rd decreased the content of lipid oxidation product MDA in the retina affected by DR (Fig. 1j). The retinal vessel morphology and perfusion were the main measures of retinal constitutive endothelial barrier stabilization, and could be detected by retinal vasculature digestion and Evans blue dye leakage assay. The administration of Rd and CaD reduced diabetes-induced retinal acellular capillary formation, and improved the vascular derangements and tortuosity (Fig. 1k and Supplementary file 1: Fig. S1k). Furthermore, there was more Evans blue extravasation in the model group, which was significantly blocked after treatment with Rd (Fig. 1l and Supplementary file 1: Fig. S1l). Moreover, therapeutic effects of Rd on in vivo BRB repair were also recapitulated in the detection of junctional proteins in the retina (Fig. 1m and Supplementary file 1: Fig. S1m-p). Similar effects were observed with the positive drug CaD, in which Rd with superior pharmacological activity and lower doses might have the better clinical potential. Above results collectively supported that Rd effectively prevented hyperglycemia-mediated retinal endothelial barrier breakdown and subsequent vascular damage both in vitro and in vivo.

Acceleration of FAO by ginsenoside Rd alleviated retinal endothelial barrier function in vivo and in vitro

Fatty acid metabolism played a multifaceted role, not only in providing energy, but also in regulating signaling pathway and endothelial function [8]. To probe the metabolic susceptibility of lipid in RVECs, a PCR screening of a panel of crucial enzymes was conducted. High glucose elicited minimal impact on fatty acid uptake (*CD36*, *FATP3* and *FATP4*), fatty acid transport (*FABP4* and *FABP5*) and fatty acid synthesis (*FASN* and *SCD1*) (Fig. S2a), but reduced transcript levels of fatty acid oxidation

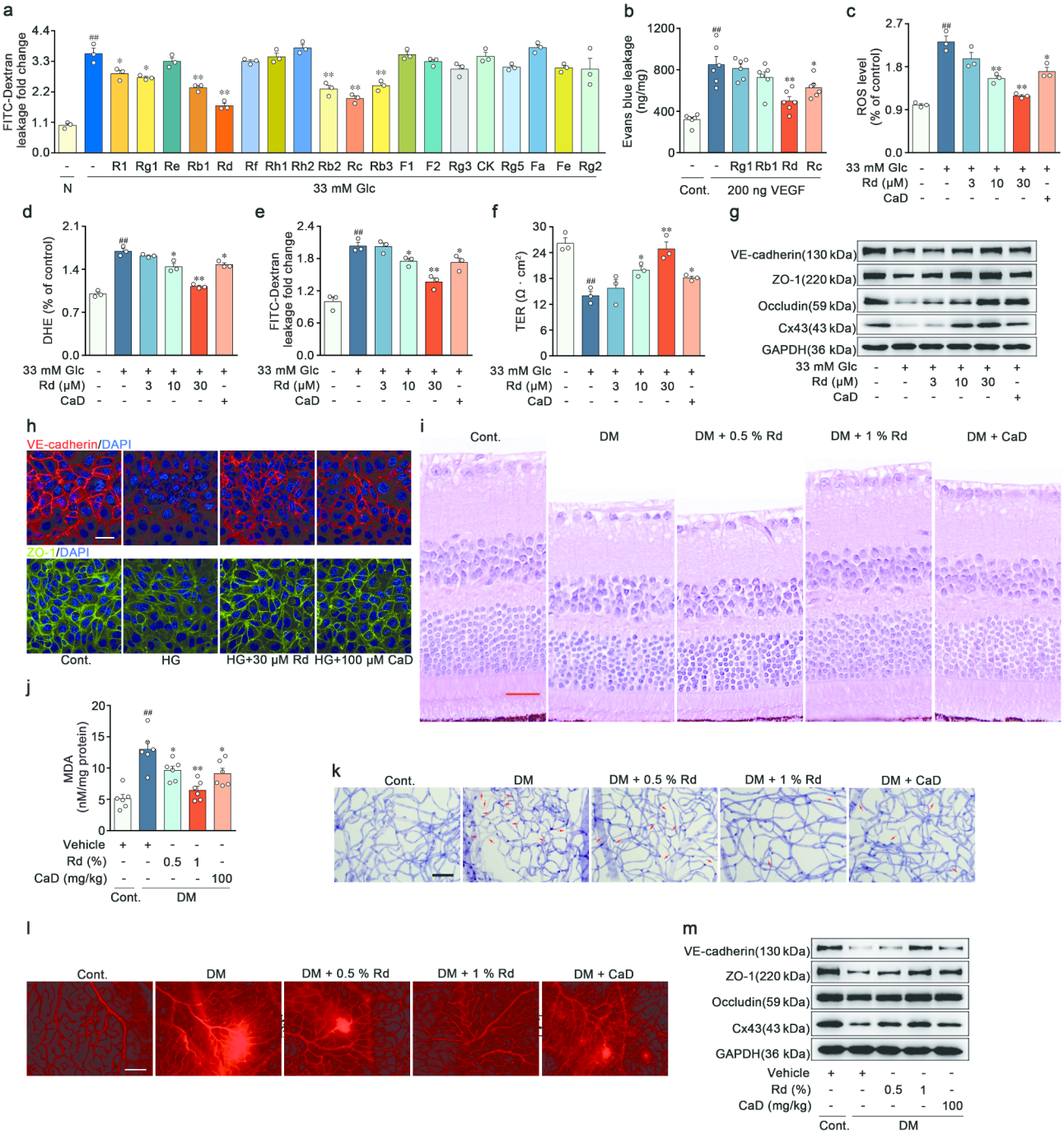

Fig. 1 Ginsenoside Rd attenuated diabetes-related endothelial barrier dysfunction in vitro and in vivo. **a** Permeability of EC monolayer was assessed by FITC-dextran. All saponins were added at a concentration of 30 μM ($n=3$). **b** Evans blue dye leakage assay was used to quantify vascular leakage in VEGF-induced acute retinal vascular hyperpermeability model by a microplate reader ($n=6$). **c-d** Mean DCFH-DA and DHE fluorescent intensity levels in RVECs treated with vehicle, high glucose (33 mM), Rd and CaD (100 μM) ($n=3$). **e-f** Endothelial monolayer integrity and polarity were examined by FITC-dextran leakage and TER assay ($n=3$). **g** Immunoblot analysis of VE-cadherin, ZO-1, Occludin and Cx43 expressions in RVECs. GAPDH was used as the loading control ($n=3$). **h** Immunofluorescent staining of VE-cadherin and ZO-1 in RVECs. Scale bars: 40 μm ($n=3$). **i** Retinal section stained with H&E. Scale bars: 25 μm ($n=5$). **j** MDA concentration of retina from vehicle, hyperglycemia, Rd-treated and CaD-treated mice ($n=6$). **k** Retinal trypsin digestion was stained with Periodic-acid Schiff's reagent. Acellular capillaries were denoted by red arrows in representative graphs. Scale bars: 50 μm ($n=5$). **l** Retinal vascular leakage in STZ-induced DR model was detected by Evans blue dye. Representative images were observed by fluorescence microscope. Scale bars: 50 μm ($n=5$). **m** Protein expressions of VE-cadherin, ZO-1, Occludin and Cx43 in retina were determined by Western blot ($n=6$). ##$p<0.01$ vs. the control, *$p<0.05$, **$p<0.01$ vs. DR group or high glucose group

(FAO) metabolic enzymes (*CPT1A* and *CPT2*) and their regulatory factors (*PPARα* and *PGC-1α*) (Fig. 2a). Mannitol was used as an osmolality control. To explore whether these transcriptional changes were accompanied by corresponding alterations in cellular metabolism, the measurements were taken by both the indirect indicator of mitochondrial FAO capacity (TMRE assay) and the direct indicator of FAO capacity (seahorse assay). There was a lower mitochondrial membrane potential in RVECs stimulated with high glucose (Fig. 2b and Fig. S2b). High glucose milieu exerted a negative effect on the palmitate oxidation rate of RVECs (Fig. 2c-d). Notably, the transcriptome data from the public database (GSE53257) supported these results, showing a downregulation of fatty acid metabolism-related processes in the retinas of DR patients (Fig. 2e). These results provided the compelling evidence implicating a decrease in FAO of ECs in response to the high glucose environment.

ECs relied on FAO to facilitate nucleotide synthesis for angiogenesis or maintain cell quiescence [24–25]. However, limited research had been performed on the relationship between FAO and endothelial permeability. To

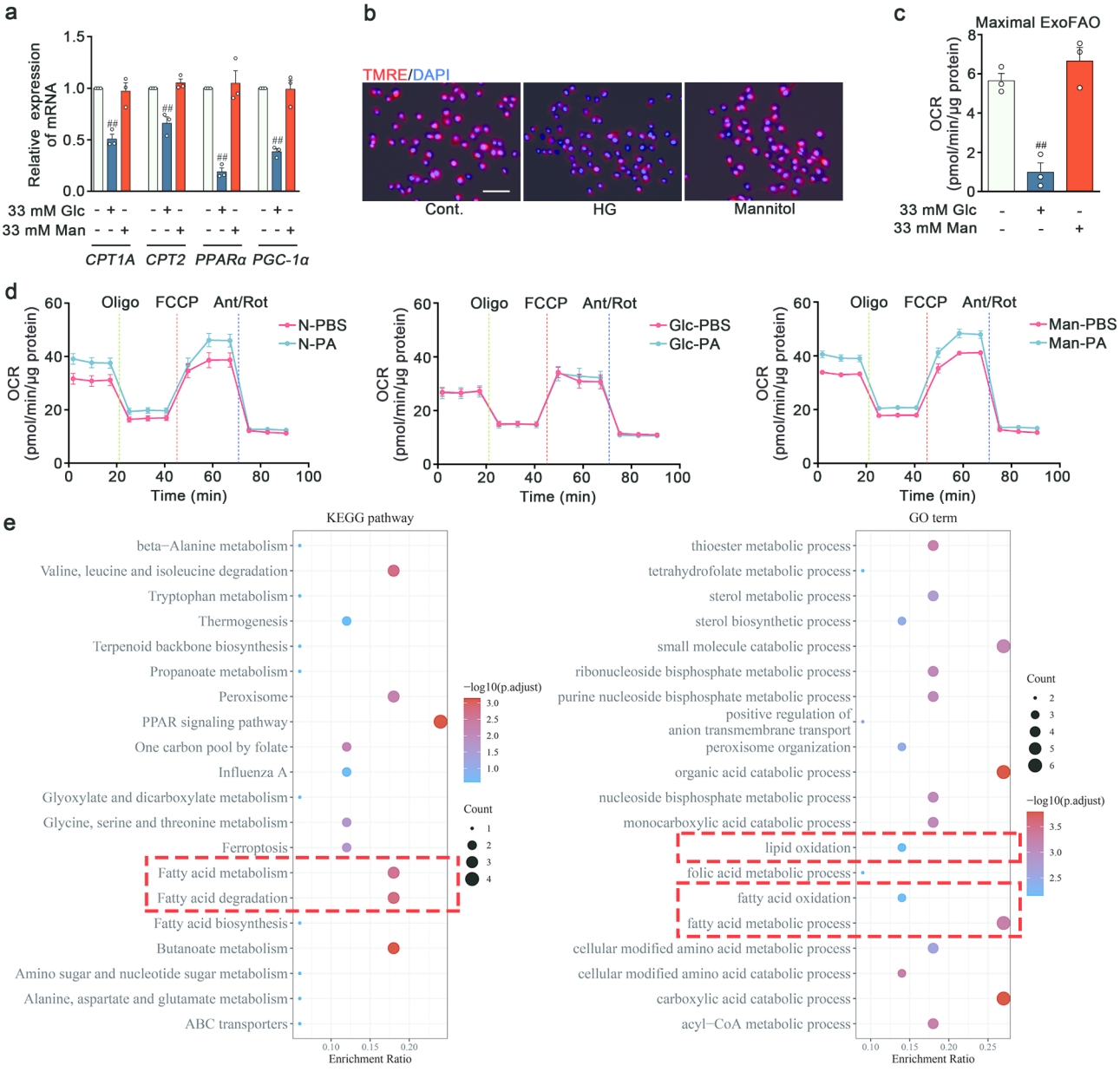

Fig. 2 High glucose diminished the endothelial capacity of FAO. **a** q-PCR analysis of *CPT1A*, *CPT2*, *PPARα* and *PGC-1α* mRNA level in RVECs treated with vehicle, high glucose and 33mM Mannitol. *GAPDH* was used as the internal reference ($n=3$). **b** Mitochondrial membrane potential was measured by TMRE fluorescent staining. Scale bars: 50 μm ($n=3$). **c-d** FAO was determined by OCR using palmitate as a substrate with Seahorse XFp Analyser ($n=3$). **e** GO and KEGG pathway enrichment analysis. ##$p<0.01$ vs. the control

ascertain whether weakened FAO was an indispensable prerequisite of BRB impairments, RVECs were treated with the PPARα agonist fenofibrate (Feb) to promote FAO. Feb inhibited ROS and MDA production (Fig. 3a-c), while preserved endothelial barrier stabilization in high glucose-induced RVECs (Fig. 3d-e). Consistently, Feb limited the loss of BRB structural proteins (VE-cadherin, ZO-1, Occludin and Cx43) (Fig. 3f-g and Fig. S2c-h). Thus, the augmented barrier permeability might be mediated by FAO in ECs.

Since the mitochondria served as the principal site for the cellular ROS generation and FAO, it was speculated that the barrier-protective activity of FAO was inextricably connected to endothelial mitochondrial ROS.

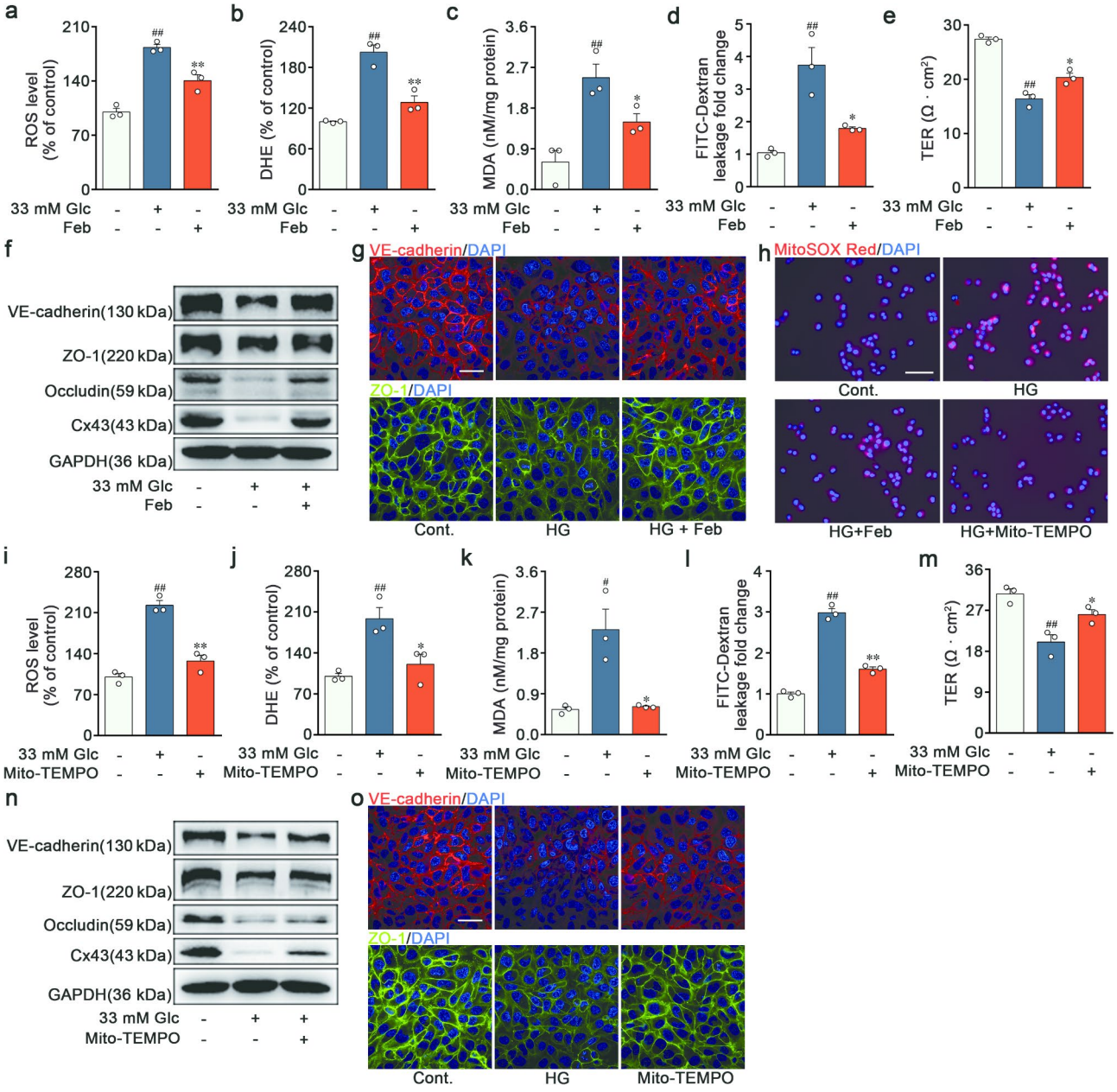

Fig. 3 High glucose drove mitochondrial oxidative stress-related endothelial dysfunction via blunting FAO in vitro. **a-c** Analysis of DCFH-DA, DHE and MDA levels in RVECs treated with vehicle, high glucose and Feb (50 μM) ($n = 3$). **d-e** FITC-dextran flux and TER of the confluent endothelial monolayer ($n = 3$). **f** Immunoblot analysis of VE-cadherin, ZO-1, Occludin and Cx43 expressions in RVECs. ($n = 3$). **g** Immunofluorescent staining of VE-cadherin and ZO-1 in RVECs. Scale bars: 40 μm ($n = 3$). **h** Mitochondrial ROS was assessed by MitoSOX staining in RVECs treated with vehicle, high glucose, Feb (50 μM) and Mito-TEMPO (50 μM). Scale bars: 50 μm ($n = 3$). **i-k** Oxidative stress assessment in RVECs ($n = 3$). **l-m** Integrity and polarity of ECs monolayer ($n = 3$). **n** Representative Western blot of VE-cadherin, ZO-1, Occludin and Cx43 in RVECs ($n = 3$). **o** Representative images of immunofluorescence for VE-cadherin and ZO-1 in RVECs. Scale bars: 40 μm ($n = 3$). #$p < 0.05$, ##$p < 0.01$ vs. the control, *$p < 0.05$, **$p < 0.01$ vs. high glucose group

High glucose contributed considerably to mitochondrial oxidative stress, indicated by MitoSOX, which was subsequently reversed by Feb and Mito-TEMPO (Fig. 3h and Fig. S2i). The mitochondrial-specific ROS scavenger, Mito-TEMPO, was found to reduce the contents of totol ROS, superoxide anion and MDA in RVECs (Fig. 3i-k), suggesting the predominant role of mitochondria-derived ROS in oxidative stress induced by high glucose. Furthermore, Mito-TEMPO enhanced the integrity and polarity of the endothelial monolayer, evidenced by the FITC-dextran leakage and TER analysis (Fig. 3l-m). Mito-TEMPO increased the expressions of junctional proteins in RVECs (Fig. 3n-o and Fig. S2j-o). The outcomes of in vivo experiments were also in agreement with the previously mentioned in vitro results, indicating the ameliorative effects of Mito-TEMPO on the retinal endothelial injury of DR (Fig. 4k-o and Fig. S3f-l). The oxidative stress, primarily caused by mitochondrial ROS, led to phenotypic and functional transitions. The above results obviously illustrated that high glucose drove mitochondrial oxidative stress-related endothelial dysfunction through the suppression of FAO.

To further identify the significance of FAO in the effectiveness of Rd against DR, the carnitine palmitoyltransferase 1 (CPT1) inhibitor etomoxir (Eto) was utilized to block FAO. Rd reciprocally mitigated the generation of total ROS, superoxide anion, MDA, and mitochondrial ROS (Fig. 4a-d and Fig. S3a). The increased endothelial monolayer permeability and the loss of junctional proteins were ameliorated by Rd in RVECs after high glucose challenge (Fig. 4e-j and Fig. S3b-e). The efficacy of Rd on mitochondrial oxidative stress-related endothelial dysfunction was largely abrogated when Eto was concurrently administered. Concordantly, Rd counteracted the retinal histopathological alterations and reinforced the expressions of VE-cadherin, ZO-1, Occludin and Cx43 in the retina of DR group. The effects of Rd were partially abolished by Eto in vivo (Fig. 4k-o and Fig. S3f-l). In accordance with these results, Rd alleviated mitochondrial oxidative stress through a FAO-associated mechanism, thereby sustaining retinal endothelial barrier function.

AMPK was activated by ginsenoside Rd through GPR30-cAMP-PKA-LKB1 pathway

Based on our previous study, Rd activated AMPK, a crucial regulatory protein for FAO, in the retinal ECs [21]. As a necessary extension of the initial study, it was postulated that AMPK might serve as the pivotal upstream regulatory molecule responsible for the vascular barrier-protective efficacy of Rd. Therefore, we sought to investigate the molecular mechanism and potential target through which Rd could activate AMPK in RVECs. Considering the structural resemblance of Rd to steroid hormones (Fig. S4l), it was plausible that Rd directly bound to steroid receptors, which could in turn phosphorylate AMPK at Thr172.

Initially, a range of steroid hormones were screened to determine the capacity for AMPK activation in RVECs. β-Estradiol, progesterone and cortisol exhibited an augmentation in AMPK phosphorylation, whereas dihydrotestosterone executed a negligible impact (Fig. 5a). RU486 (progesterone and glucocorticoid receptor antagonist) was found to have no effect on the ability of Rd to activate AMPK (Fig. 5b). Unexpectedly, the estrogen receptor (ER) antagonist ICI182780 intensified Rd's facilitation of phosphorylated AMPK (Fig. 5b). ER comprises both the nuclear receptor family (ERα and ERβ) and membrane receptor family (GPR30). Previous studies indicated that ICI182780 was commonly used as an antagonist for ERα and ERβ, but it could also act as an agonist for GPR30 [26]. Despite the fact that G1 (a GPR30-specific agonist) promoted AMPK activation, the GPR30 antagonist G15 (1 μM) was not available to attenuate the activity of Rd (Fig. 5c). G15 was reported as a partial agonist for ERα at high concentrations, and β-estradiol increased p-AMPK levels through its binding to ERα [26]. As anticipated, there was a marked inhibition of Rd-induced AMPK activation when the concentration of G15 was decreased to 10 nM (Fig. 5d and Fig. S4a). In addition, the ERα-specific antagonist MPP or the ERβ-specific antagonist PHTPP failed to diminish the effects of Rd (Fig. 5d and Fig. S4a). The effective concentrations of a tested drug might result in nonclassic or biphasic dose responses in pharmacological reactions related to steroid receptors, involving receptor selectivity, cross-reactivity, and multiple signaling pathways. These results proved that AMPK phosphorylation induced by Rd was dependent on the activation of GPR30.

The activation of GPR30 exerted biological effects through various kinase-signaling cascades. Both Rd and G1 elevated intracellular cAMP levels in RVECs, whereas the cAMP accumulation resulting from Rd was regressed by G15 or *GPR30* knockdown (Fig. 5e-f). Concomitantly, Rd and G1 induced notable phosphorylation of PKA, which was then believed to activate LKB1 and hence stimulate AMPK activity (Fig. 5d and Fig. S4b-c). Rd enhanced the activation of LKB1 and AMPK, but this effect was abrogated when RVECs were pretreated with adenylate cyclase inhibitor (SQ22536), cAMP competitive antagonist (Rp-cAMPs) or PKA inhibitor (H-89). As a positive control, the adenylate cyclase activator forskolin elicited a similar effect compared to Rd (Fig. 5g and Fig. S4d-e). Furthermore, knockdown of *LKB1* decreased the action of Rd on phosphorylation of AMPK (Fig. 5h). Rd improved the levels of p-PKA, p-LKB1, and p-AMPK in RVECs, regardless of the presence of MPP or PHTPP. By contrast, the pharmacological

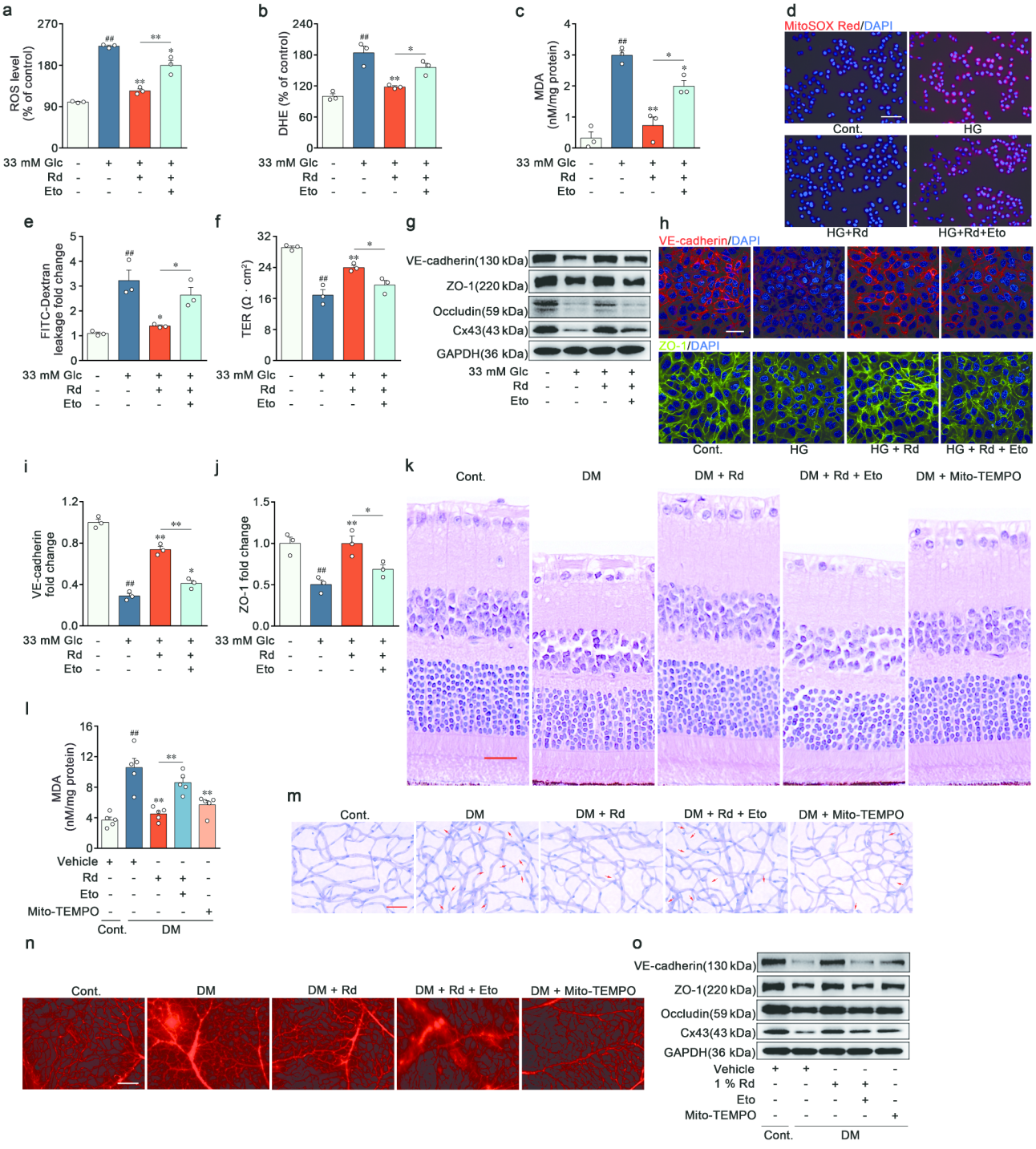

Fig. 4 Ginsenoside Rd alleviated impaired retinal endothelial barrier function via acceleration of FAO in vivo and in vitro. **a-c** Quantitative analysis of DCFH-DA, DHE and MDA levels in RVECs treated with vehicle, high glucose, Rd (30 μM) and Eto (40 μM) ($n = 3$). **d** Mitochondrial ROS was assessed by Mito-SOX staining. Scale bars: 50 μm ($n = 3$). **e-f** Integrity and polarity of ECs monolayer ($n = 3$). **g** Immunoblot analysis of VE-cadherin, ZO-1, Occludin and Cx43 expressions in RVECs ($n = 3$). **h-j** Immunofluorescent staining of VE-cadherin and ZO-1 in RVECs. Scale bars: 40 μm ($n = 3$). **k** Retinal section stained with H&E. Scale bars: 25 μm ($n = 5$). **l** MDA concentration of retinal sections ($n = 5$). **m** Retinal trypsin digestion and staining. Acellular capillaries were denoted by red arrows in representative graphs. Scale bars: 50 μm ($n = 5$). **n** Retinal vascular leakage of Evans blue dye. Scale bars: 50 μm ($n = 5$). **o** Proteins levels of VE-cadherin, ZO-1, Occludin and Cx43 in retina were determined by Western blot ($n = 6$). ##$p < 0.01$ vs. the control, *$p < 0.05$, **$p < 0.01$ vs. DR group, high glucose group or the indicated group

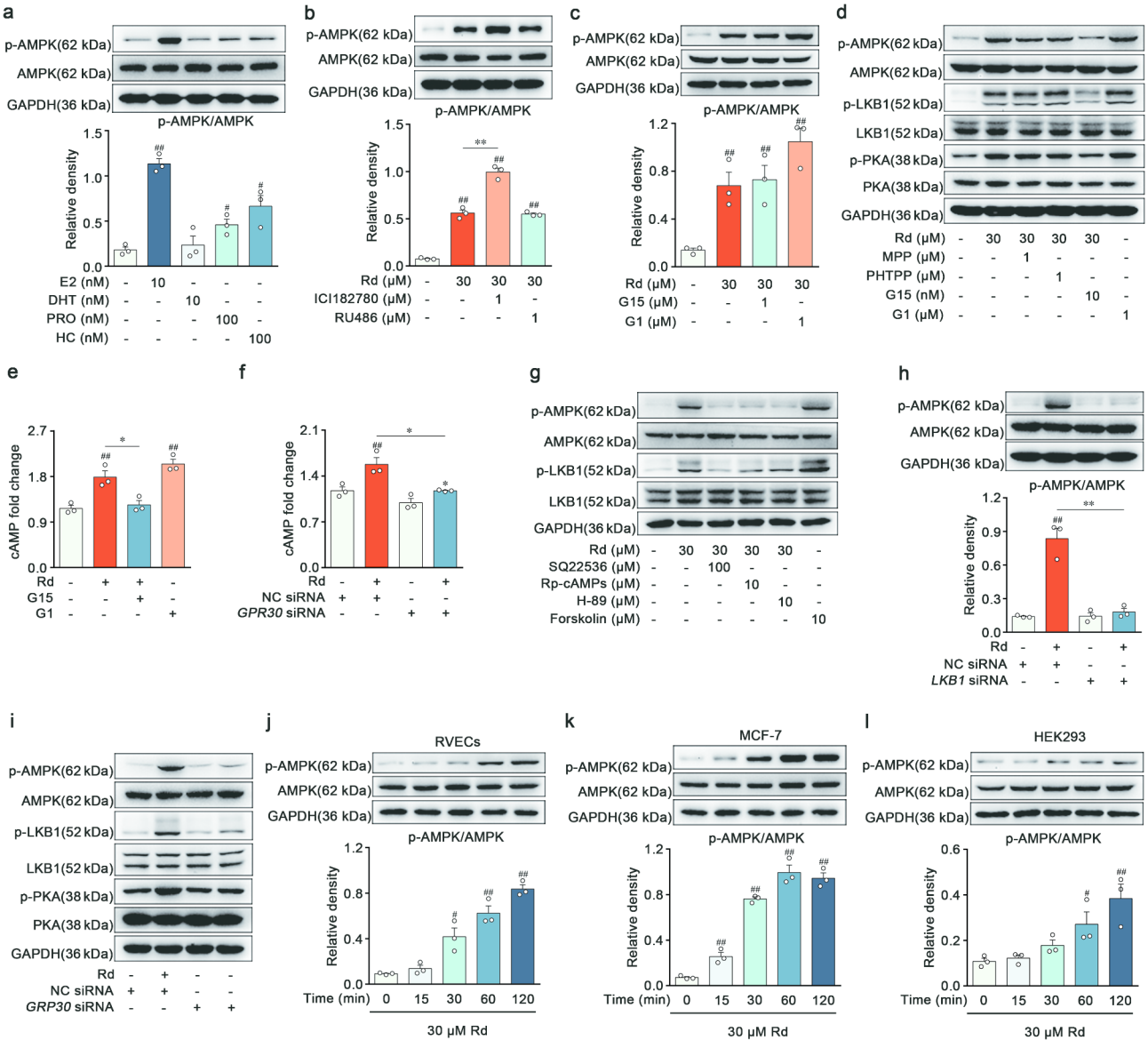

Fig. 5 AMPK was activated by ginsenoside Rd through GPR30-cAMP-PKA-LKB1 pathway. **a** Immunoblot analysis of p-AMPK and AMPK in RVECs treated with vehicle, 10 nM β-estradiol (E2), 10 nM dihydrotestosterone (DHT), 100 nM progesterone (PRO) and 100 nM cortisol (hydrocortisone, HC) ($n = 3$). **b** Immunoblot analysis of p-AMPK and AMPK in RVECs treated with vehicle, 30 μM Rd, 1 μM ICI182780 and 1 μM RU486 ($n = 3$). **c** Protein level of p-AMPK and AMPK were determined by Western blot in RVECs treated with vehicle, 30 μM Rd, 1 μM G15 and 1 μM G1 ($n = 3$). **d** Representative Western blot of p-AMPK, AMPK, p-LKB1, LKB1, p-PKA and PKA in RVECs treated with vehicle, 30 μM Rd, 1 μM MPP, 1 μM PHTPP, 10 nM G15 and 1 μM G1 ($n = 3$). **e-f** cAMP levels were analyzed in RVECs ($n = 3$). **g** Western blot analyzed the protein level of p-AMPK, AMPK, p-LKB1 and LKB1 in RVECs treated with vehicle, 30 μM Rd, 100 μM SQ22536, 10 μM Rp-cAMPs, 10 μM H-89 and 10 μM forskolin ($n = 3$). **h** Immunoblot analysis of p-AMPK and AMPK in RVECs treated with vehicle, 30 μM Rd, NC siRNA and *LKB1* siRNA ($n = 3$). **i** Representative Western blot of p-AMPK, AMPK, p-LKB1, LKB1, p-PKA and PKA in RVECs treated with vehicle, 30 μM Rd, NC siRNA and *GPR30* siRNA ($n = 3$). **j-l** Protein level of p-AMPK and AMPK were determined by Western blot in RVECs, MCF-7, and HEK293 ($n = 3$). #$p < 0.05$, ##$p < 0.01$ vs. the control, *$p < 0.05$, **$p < 0.01$ vs. Rd group or the indicated group

inhibition or genetic suppression of GPR30 reversed these alternations caused by Rd (Fig. 5d, i, Fig. S4a-c and f-h). To further substantiate the essential of GPR30 in the AMPK pathway activated by Rd, we examined the time-dependent induction of AMPK activation in RVECs (low GPR30 expression), MCF-7 (high GPR30 expression), and HEK293 (no GPR30 expression) (Fig. S4i). The increase in p-AMPK generated by Rd was directly proportional to the abundance of GPR30 in the tested cell lines (Fig. 5j-l). Validations of siRNA knockdown for *GPR30* and *LKB1* were shown in Fig. S4j-k. These aforementioned pharmacological studies unequivocally suggested that Rd activated the signaling pathway composed of GPR30-cAMP-PKA-LKB1-AMPK.

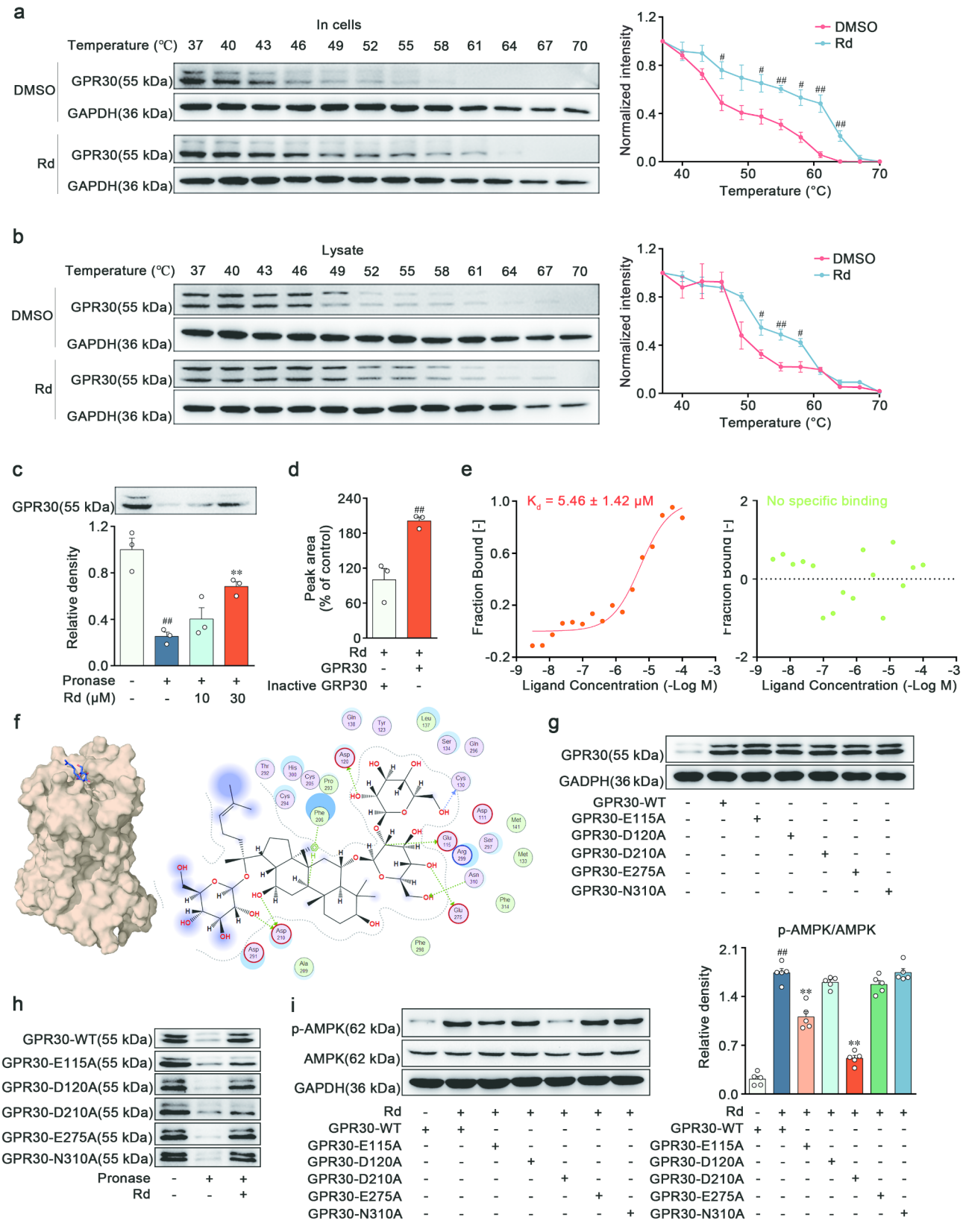

Fig. 6 (See legend on next page.)

(See figure on previous page.)

Fig. 6 GPR30 was identified as a target protein binding with ginsenoside Rd. **a-b** Thermal stability of GPR30 in intact RVECs and cell lysates treated with vehicle and 30 μM Rd was measured by the CETSA ($n=3$). **c** Stability of GPR30 against enzymatic hydrolysis in RVECs lysates treated with vehicle and Rd was measured by the DARTS ($n=3$). **d** Affinity between GRP30 and Rd was tested by HPLC-QQQ-MS/MS ($n=3$). **e** Binding affinity of Rd with GPR30 was determined by the MST. An empty vector that only expresses EGFP was included as negative controls ($n=3$). **f** Docking of protein GPR30 and Rd. **g** Overexpression of GPR30 was verified by Western blot ($n=3$). **h** Immunoblotting analysis of the binding between 30 μM Rd and GPR30 with different mutations by DARTS in HEK293T ($n=3$). **i** Immunoblot analysis of p-AMPK and AMPK ($n=3$). #$p<0.05$, ##$p<0.01$ vs. the control, **$p<0.01$ vs. Pronase group or Rd-treated group

GPR30 was identified as a target protein binding with ginsenoside Rd

Because Rd had no effect on the endogenous expression of GPR30 in RVECs (Fig. S5a), the investigation aimed to determine the binding characteristics of Rd and GPR30 using the thermodynamic and kinetic experiments. Upon binding to small molecule, conformational changes of the target protein occurred, leading to the alterations in protein stability. Firstly, the incubation with Rd stabilized GPR30 in heat-denatured intact RVECs and cell lysates for the cellular thermal shift assay (CETSA) (Fig. 6a-b). On the drug affinity responsive target stability assay (DARTS), the stability of GPR30 against enzymatic hydrolysis in RVECs lysates was improved by Rd in a concentration-dependent manner (Fig. 6c). Another indirect method for assessing binding was affinity ultrafiltration mass spectrometry. This technique involved separating ligand-protein complexes from free components using ultrafiltration, and then analyzing the released ligands (Rd) using LC-MS. The resultant increase in the MS response indirectly confirmed the binding between Rd and GPR30 (Fig. 6d and Fig. S5b). On the microscale thermophoresis assay (MST), the recorded equilibrium dissociation constant was rated at approximately 5.46 μM, indicative of Rd's feasible binding affinity with GRP30, and Rd failed to combine with negative control with EGFP (Fig. 6e). The results of molecular docking predicted that Rd and the amino acid residues of Glu 115, Asp 120, Asp 210, Glu 275, and Asn 310 of GPR30 could form hydrogen bonds, in which these predicted amino acid residues were located in the native ligand binding pocket of GPR30 (Fig. 6f). To further validate these sites, the site-directed mutations were conducted and the overexpression of GPR30 was verified (Fig. 6g). The results of DARTS assay demonstrated that the mutating sites of Asp 120, Glu 275, and Asn 310 by alanine did not affect the interaction, but the mutating sites of Glu 115 and Asp 210 by alanine diminished the binding between Rd and GPR30 (Fig. 6h). Meanwhile, the mutations of Glu 115 and Asp 210 compromised the AMPK activation induced by Rd (Fig. 6i), and Glu 115 and Asp 210 of GPR30 are conserved in species ranging from *Homo sapiens* to various mammals (Fig. S5c). Therefore, the key residues of Glu 115 and Asp 210 were responsible for the interaction of Rd and GPR30. Collectively, the accumulated data definitively situated GPR30 as a direct target of Rd.

Ginsenoside Rd restored high glucose-induced FAO defect and endothelial barrier dysfunction via GPR30-AMPK pathway

After unearthing the target and upstream regulatory mechanism of Rd, the subsequent objective was to elucidate the potential impact of the GPR30-AMPK cascade on downstream phenotypic and functional outcomes. Rd and G1 potentiated the phosphorylation of AMPK and ACC, the expressions of PGC-1α and PPARα, and the mRNA levels of *CPT1A*, *CPT2*, *PGC-1α* and *PPARα* in RVECs treated with high glucose (Fig. 7a-b and Fig. S6a-d). ACC converted acetyl-CoA to malonyl-CoA, which served as a physiological inhibitor of CPT1A, the decisive rate-limiting enzyme in FAO. AMPK-triggered ACC phosphorylation could inhibit the catalytic activity [27]. Additionally, AMPK modulated the transcription of metabolic enzyme in FAO through the transcription factors, PGC-1α and PPARα. Rd and G1 magnified maximal oxygen consumption rate (OCR) change resulting from exogenous FAO and increased the mitochondrial membrane potential (Fig. 7c-d and Fig. S6e-f). However, the stimulation of Rd on fatty acid metabolism pathway and flux of FAO were diminished by the GPR30 antagonist G15 and AMPK inhibitor Compound C (C-C) (Fig. 7a-d and Fig. S6a-f). These results strongly provided evidence for the accelerative ability of Rd on high glucose-impaired FAO via the GPR30-AMPK-ACC-CPT1A/PGC-1α-PPARα axis. Consistently, Rd and G1 suppressed high glucose-driven mitochondrial oxidative stress and dissolution of inter-endothelial junctions. Conversely, the pharmacological blockage of GPR30 and AMPK using G15 and C-C elicited weakening effects on pharmacodynamics of Rd, including anti-mitochondrial oxidative stress (Fig. 7e-h and Fig. S6g), increased endothelial integrity (Fig. 7i-j) and emphasis on barrier proteins (Fig. 7k-l and Fig. S6h-m). Together, these results corroborated the function for GPR30-AMPK pathway in the efficacy of Rd in mitigating FAO deficiency and endothelial barrier dysfunction.

AMPK supported IDH2-catalyzed mitochondrial NADPH regeneration to maintain redox homeostasis in a FAO-dependent manner

The BRB injury was primarily contributed by the endothelial mitochondrial ROS, with FAO being the main source of endothelial mitochondrial respiration rather than glycolysis [28]. It was speculated that compromised FAO might be the reason for endothelial mitochondrial

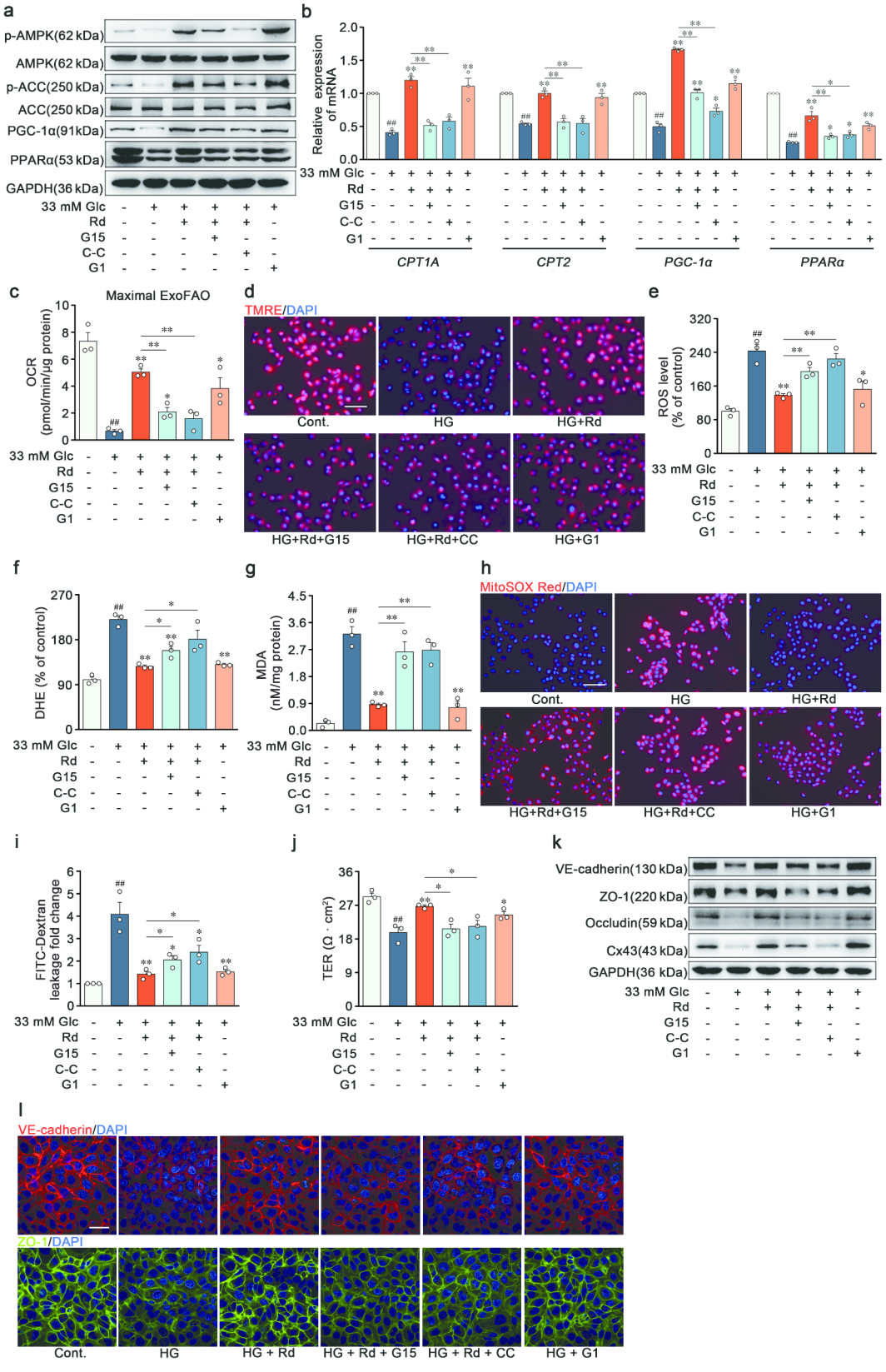

Fig. 7 (See legend on next page.)

(See figure on previous page.)

Fig. 7 Ginsenoside Rd restored high glucose-induced FAO defect and endothelial barrier dysfunction via GPR30-AMPK pathway. **a** Immunoblot analysis of p-AMPK, AMPK, p-ACC, ACC, PGC-1α and PPARα expressions in RVECs treated with vehicle, high glucose, 30 μM Rd, 10 nM G15, 1 μM C-C and 1 μM G1 ($n=3$). **b** mRNA relative expressions of *CPT1A*, *CPT2*, *PGC-1α* and *PPARα* were measured by qRT-PCR ($n=3$). **c** Bar chart showing maximal OCR alterations due to exogenous FAO ($n=3$). **d** TMRE fluorescence images of RVECs treated with vehicle, high glucose, Rd, G15, C-C and G1. Scale bars: 50 μm ($n=3$). **e-g** Quantitative analysis of DCFH-DA, DHE, and MDA levels in RVECs ($n=3$). **h** Mitochondrial ROS levels were evaluated in RVECs using MitoSOX. Scale bars: 50 μm ($n=3$). **i-j** Integrity and polarity of ECs monolayer ($n=3$). **k** Immunoblot analysis of VE-cadherin, ZO-1, Occludin and Cx43 expressions in RVECs ($n=3$). **l** Immunofluorescent staining of VE-cadherin and ZO-1 in RVECs. Scale bars: 40 μm ($n=3$). ##$p<0.01$ vs. the control, *$p<0.05$, **$p<0.01$ vs. high glucose group or the indicated group

oxidative stress after exposure to high glucose. Mitochondrial ROS levels were meticulously monitored by an intricate and orchestrated system of antioxidant defense mechanisms [29]. Therein, manganese superoxide dismutase (Mn-SOD), which was exclusively localized in mitochondrial matrix, catalyzed the conversion of superoxide into hydrogen peroxide (H_2O_2). Nicotinamide adenine dinucleotide phosphate (NADPH) was physiologically coupled with glutathione (GSH) pool and strictly scavenged peroxide. Rd preserved the contents of NADPH and GSH, as well as the activity of Mn-SOD in RVECs after high glucose challenge, while those alternations were abolished by AMPK inhibitor C-C (Fig. 8a-c). Due to the inability of NADPH to penetrate the mitochondrial membrane, the mRNA levels of the key enzymes responsible for mitochondrial NADPH regeneration were measured. There were no significant responses observed in *MTHFD1*, *ME2*, *ME3*, *GLUD* and *NNT*, but high glucose reduced the transcripts of *MTHFD2* and *IDH2* in RVECs (Fig. 8d). Rd was ineffective to *MTHFD2* mRNA levels, but revitalized the expression of IDH2 in an AMPK-dependent manner (Fig. S7a-b). IDH2 was crucial for Rd to sustain the mitochondrial NADPH pool.

In cancer cells, IDH2 levels increased adaptively upon metabolic stress via the AMPK-FOXO1 pathway [30]. Rd led to drastic AMPK activation, which in turn triggered the nuclear translocation of FOXO1 (Fig. 8e and Fig. S7c). ChIP assay suggested that FOXO1 antibody could expectedly enrich the DNA of *IDH2* promoter region, and Rd strengthened the binding of FOXO1 to *IDH2* promoter, which was disrupted by C-C (Fig. 8f). Beyond the transcriptional control of gene expression, the enzymatic activity of IDH2 could also be regulated by post-translational modifications. High glucose decreased the expression of mitochondrial deacetylase SIRT3 and increased the levels of acetylated inactive form of IDH2. And Rd reduced the levels of acetylated IDH2 by enhancing the interaction with SIRT3 and IDH2 (Fig. 8g and Fig. S7d-f). As reported in the literature, PGC-1α polymerized with ERRα enriched the *SIRT3* promoter region [31]. After demonstrating the transcriptional augmentation of *SIRT3* by Rd, C-C and Compound A (C-A) were employed to inhibit AMPK and ERRα respectively, and the treatment blocked the enhancing effects of Rd (Fig. 8h). Similarly, Rd reversed the activity of mitochondrial IDH in high glucose-stimulated RVECs, while this change was suppressed by SIRT3 inhibitor 3-TYP, FOXO1 inhibitor AS1842856 and C-C (Fig. 8i). Concordantly, the regulation of Rd on total ROS (Fig. 8j), superoxide anion (Fig. 8k), MDA (Fig. 8l), mitochondrial NADPH (Fig. 8m), mitochondrial GSH (Fig. 8n) and mitochondrial ROS (Fig. 8o and Fig. S7g) were lost when co-incubation with 3-TYP or AS1842856. Similar to IDH2, Mn-SOD could be deacetylated and potentiated by SIRT3. The activation of Mn-SOD was observed following the treatment with Rd, and further hampered by 3-TYP or C-A (Fig. 8p). The TCA cycle metabolite isocitrate served as the substrate for the oxidative decarboxylation reaction catalyzed by IDH2 to regenerate NADPH from $NADP^+$. Therefore, TCA cycle influenced the rate of $NADP^+$ reduction mediated by IDH2, and acetyl-CoA (Ac-CoA) from FAO could satisfy the demands of TCA pathway. As shown in the ELISA assay and metabolite determination by LC-MS, Rd accelerated AMPK-related FAO, which was accompanied by the elevated concentrations of TCA cycle intermediates (Ac-CoA, citric acid, cis-aconitic acid, α-ketoglutaric acid, succinic acid, fumaric acid, L-malic acid, and oxaloacetic acid) (Fig. S7h). Moreover, *IDH2* knockdown partly weakened the ability of Rd to ameliorate mitochondrial oxidative stress (Fig. 8q and Fig. S8a-f), endothelial barrier compromise (Fig. 8r-s), and junctional proteins loss (Fig. 8t and Fig. S8g-m). The results of siRNA-mediated knockdown of *IDH2* was seen in Fig. S8n. The *IDH2* overexpression recapitulated the observed phenotype in Rd, encompassing mitochondrial redox homeostasis (Fig. 8u and Fig. S9a-f) and vascular barrier enhancement (Fig. 8v-x and Fig. S9g-m). The overexpression of *IDH2* was validated by Western blot (Fig. S9n).

As articulated in Fig. 8y, AMPK activated by Rd supported mitochondrial NADPH regeneration to maintain redox homeostasis and repair BRB breakdown by the FOXO1-dependent transcription of *IDH2*, SIRT3-dependent deacetylation of IDH2, and FAO-dependent growth of TCA cycle flux.

Ginsenoside Rd ameliorated lipid metabolism disorders and vascular barrier damage by targeting GPR30 in the retina of diabetic mice

To interrogate whether the activation of GPR30 underlay the therapeutic efficacy of Rd on BRB stabilization in vivo, a model of retinal *GPR30*-knockdown mice was

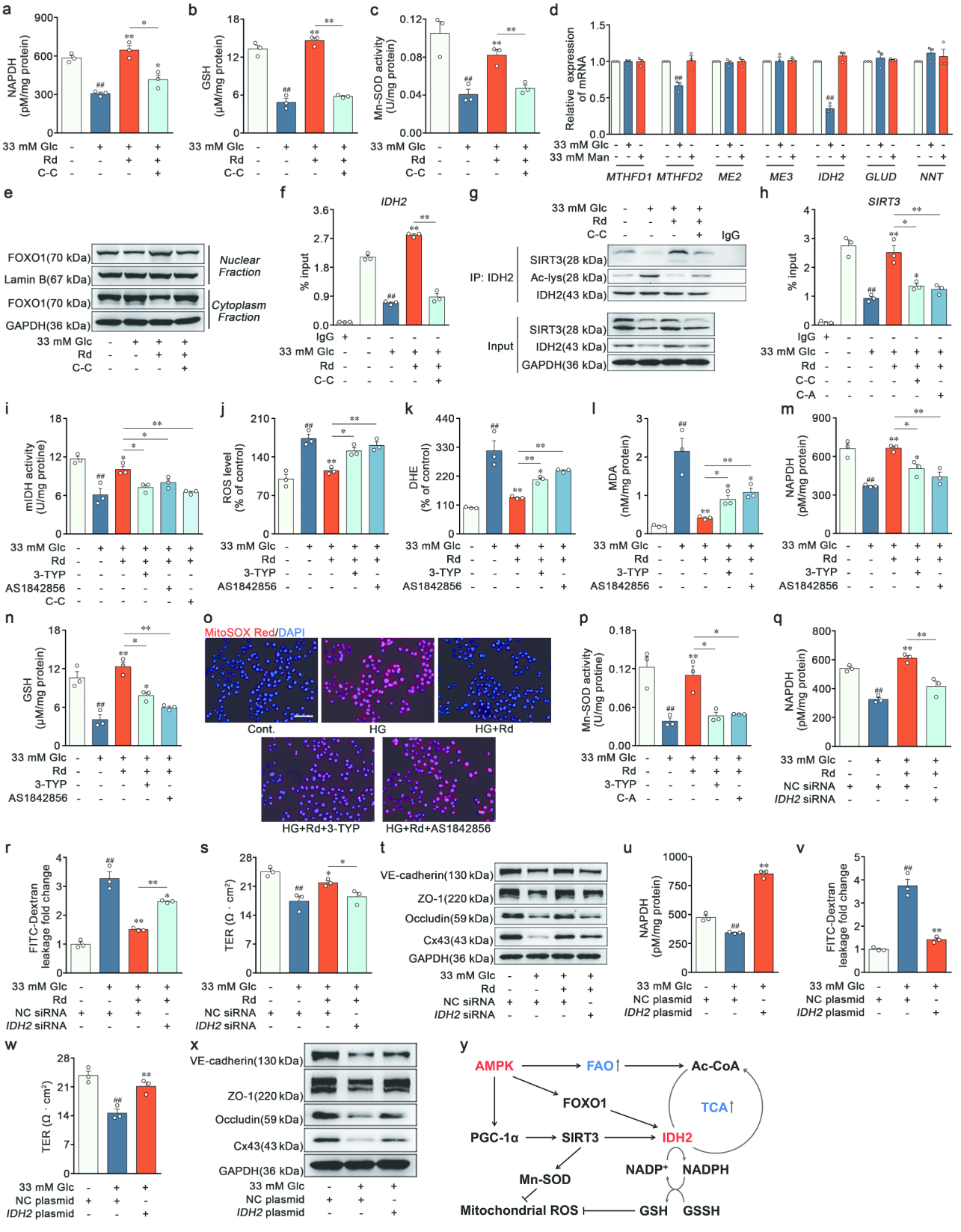

Fig. 8 (See legend on next page.)

(See figure on previous page.)

Fig. 8 AMPK supported IDH2-catalyzed mitochondrial NADPH regeneration to maintain redox homeostasis in a FAO-dependent manner. **a-b** Mitochondrial NADPH and GSH abundance in vehicle, high glucose, 30 μM Rd and 1 μM C-C-treated RVECs ($n=3$). **c** Enzymatic activity of Mn-SOD in RVECs stimulated with vehicle, high glucose, Rd and C-C ($n=3$). **d** Screening for critical enzymes of mitochondrial NADPH regeneration by qPCR ($n=3$). **e** Immunoblotting analysis of nuclear and cytosolic FOXO1 in RVECs. Lamin B was used as the nuclear loading control and GAPDH as the cytosolic loading control ($n=3$). **f** Analysis of FOXO1 on *IDH2* promoter by ChIP-qPCR ($n=3$). **g** Immunoprecipitation of IDH2 was performed to detect the combination of IDH2 and SIRT3 ($n=3$). **h** Analysis of PGC-1α on *SIRT3* promoter by ChIP-qPCR ($n=3$). **i** Enzymatic activity of mIDH in RVECs stimulated with vehicle, high glucose, 30 μM Rd, 5 μM 3-TYP, 5 μM AS1842856 and 1 μM C-C ($n=3$). **j-l** Quantitative analysis of DCFH-DA, DHE and MDA levels in RVECs ($n=3$). **m-n** Mitochondrial NADPH and GSH contents in RVECs ($n=3$). **o** Mitochondrial ROS levels were evaluated in RVECs. Scale bars: 50 μm ($n=3$). **p** Mn-SOD activity was determined in RVECs stimulated with vehicle, high glucose, 30 μM Rd, 5 μM 3-TYP and 1 μM C-A ($n=3$). **q** Content of mitochondrial NADPH in RVECs with control transfection or *IDH2* knockdown and treated with vehicle, high glucose and 30 μM Rd ($n=3$). **r-s** Integrity and polarity of ECs monolayer with *IDH2* knockdown ($n=3$). **t** Immunoblot analysis of VE-cadherin, ZO-1, Occludin and Cx43 expressions in RVECs with *IDH2* knockdown ($n=3$). **u** Mitochondrial NADPH regeneration increased in RVECs transfected with *IDH2* plasmid ($n=3$). **v-w** Detection of FITC-dextran leakage and TER of RVECs monolayer with *IDH2* plasmid ($n=3$). **x** VE-cadherin, ZO-1, Occludin and Cx43 expressions were detected by Western blot in RVECs with *IDH2* plasmid ($n=3$). **y** Mechanism schematic of the AMPK-driven redox homeostasis in RVECs. ##$p<0.01$ vs. the control, *$p<0.05$, **$p<0.01$ vs. high glucose group or the indicated group

created by intravitreal injection of adeno-associated virus (AAV8-sh*GPR30*). The successful inhibition of GPR30 in the retina was confirmed through the Western blot (Supplementary file 1: Fig. S10a). Pathological staining revealed that Rd was effective in mitigating disorganization of retinal anatomy in response to hyperglycemia, and elicited minimal effects on AAV8-sh*GPR30* mice. In contrast, retinal structural features remained stable between Rd and AAV8-NC shRNA co-treatment groups (Fig. 9a and Supplementary file 1: Fig. S10b). Under prolonged hyperglycemic conditions, Rd triggered a decrease in capillary degeneration coupled with reduced extravasation of Evans blue, and a decline in the expression of junctional proteins (VE-cadherin, ZO-1, Occludin and Cx43) in the retina. However, these effects were notably attenuated in mice treated with AAV8-sh*GPR30*, compared with those treated with AAV8-NC shRNA (Fig. 9b-c, h, Supplementary file 1: Fig. S10c-d and l-o). While observing retinal ultrastructure using transmission electron microscopy (TEM), control mice exhibited retinal capillaries with a normal and uninterrupted tight junctions (yellow arrow). Hyperglycemia disrupted the electron-dense region indicative of the tight junctions, and punctuated endothelial barrier (red arrow) (Fig. 9d). After diabetic induction, retinal ganglion cells displayed unclear and incomplete nuclear membranes (red star), chromatin dissolution (green star), and neuropil edema (blue star) (Fig. 9e). Additional anomalies including nuclear pyknosis of the bipolar cell (green arrow) and boosted cell cavity voids (red arrow) were identified in the retinal inner nuclear layer of the model mice (Fig. 9f). The outer segments of diabetic individuals revealed a reduction in photoreceptor extracellular membrane disks length, alongside a disorganized structure characterized by swelling, degeneration, and vacuoles (Fig. 9g). The above detrimental changes in the capillary, ganglion, inner nuclear layer and outer segments were uniformly prevented by the application of Rd in the retina of DR mice. Conversely, the advancement of such therapeutic alterations of Rd was absent during concurrent administration of Rd and AAV8-sh*GPR30* in the tested retinas (Fig. 9d-g).

For in vivo mechanism validation, Rd expectedly phosphorylated AMPK and ACC, and preserved the levels of CPT1A, PPARα and PGC-1α (Fig. 9h and Supplementary file 1: Fig. S10e-i). Meanwhile, Rd reversed the elevated contents of MDA (Fig. 9i), and reduced levels of NADPH (Fig. 9j) and GSH (Fig. 9k) in retina. The downregulation of IDH2 and SIRT3 in response to hyperglycemia were restored by Rd (Fig. 9h and Supplementary file 1: Fig. S10j-k). Concordantly, the beneficial effects of Rd on FAO defect and oxidative stress were approximately abolished by *GPR30* knockdown (Fig. 9h-k and Supplementary file 1: Fig. S10e-k). Similar to Rd, the GPR30 agonist G1 exerted an increased retinal resistance to hyperglycemia stimulation and repaired the pathological changes in DR, providing additional evidence to support our hypothesis (Fig. 9a-k and Supplementary file 1: Fig. S10b-o). Taken together, these results underscored the critical role of Rd in ameliorating abnormal redox status and subsequent BRB collapse by intervening GPR30-driven FAO.

Discussion

DR can be managed through various treatment modalities, including intraocular injection of glucocorticoids, vitrectomy, retinal laser photocoagulation and intravitreal injections of anti-VEGF agents. The current first-line therapies are primarily applicable for advanced DR, but which are associated with numerous notable limitations [32]. Among them, targeting VEGF treatment has demonstrated encouraging clinical advantages by mitigating the risk of neovascularization and retinal detachment. The blockade of single target may appear appealing, but could trigger compensatory regulation in a complex disease of multifactorial basis, which is the main reason for resistance or nonresponse [33–34]. Given that a significant portion of detrimental alterations in advanced DR are irreversible, early systematic detection and timely prevention are crucial for preventing vision impairment in DR patients. The sole recognized clinical intervention for early DR is the control of hyperglycemia,

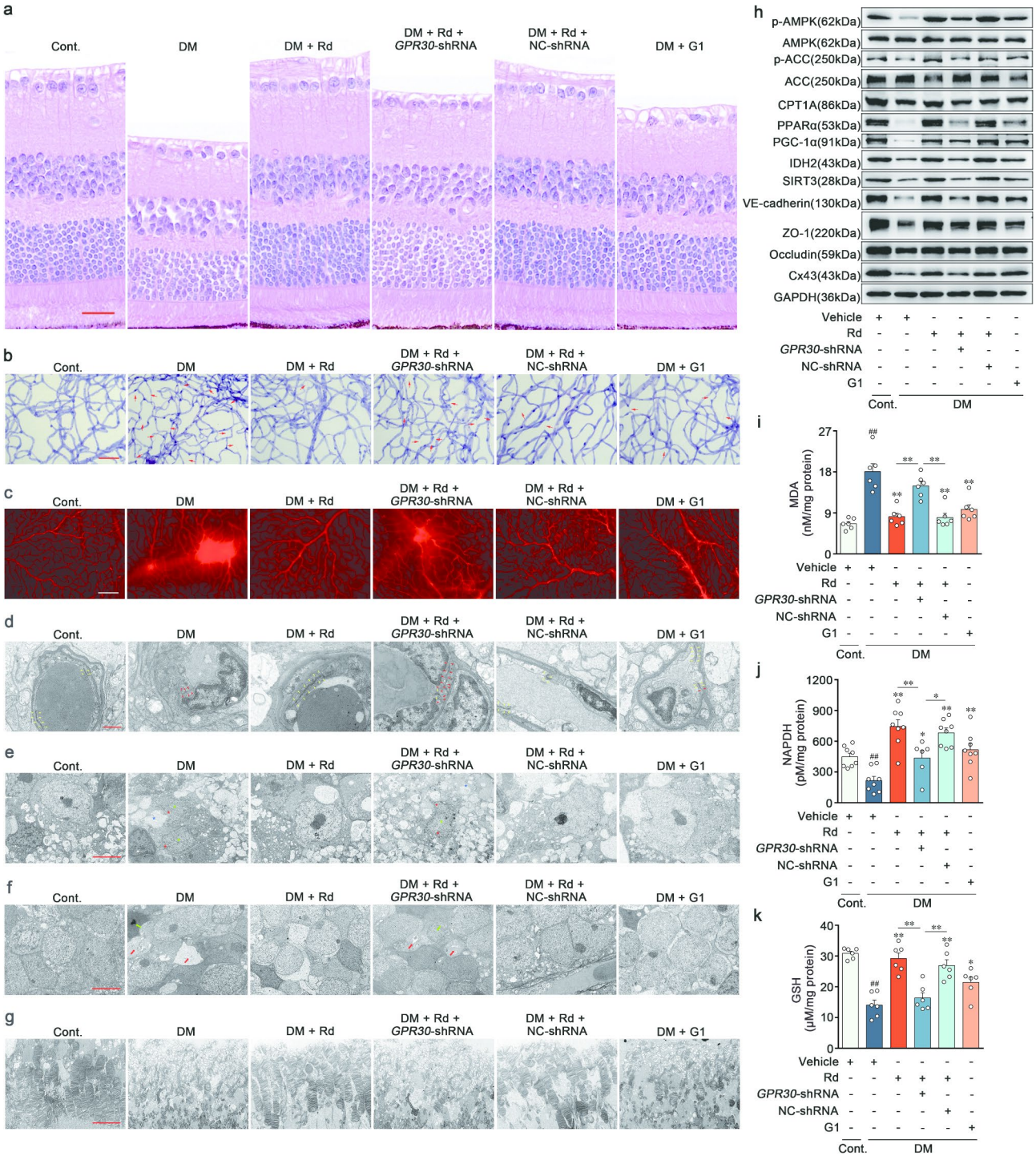

Fig. 9 Ginsenoside Rd ameliorated lipid metabolism disorders and vascular barrier damage by targeting GPR30 in the retina of diabetic mice. **a** Representative images of H&E staining. Scale bars: 25 μm ($n=5$). **b** Representative images of PAS staining in retinal vascular network. Acellular capillaries were denoted by red arrows. Scale bars: 50 μm ($n=6$). **c** Representative images of retinal Evans blue leakage in all experiment groups. Scale bars: 50 μm ($n=6$). **d** Electron micrograph of retinal capillary. Scale bars: 1 μm ($n=6$). **e** Electron micrograph of retinal ganglion cells. Scale bars: 5 μm ($n=6$). **f** Electron micrograph of bipolar cells in inner nuclear layer. Scale bars: 5 μm ($n=6$). **g** Electron micrograph of photoreceptor extracellular membrane disk. Scale bars: 5 μm ($n=6$). **h** Immunoblot analysis of p-AMPK, AMPK, p-ACC, ACC, CPT1A, PPARα, PGC-1α, IDH2, SIRT3, VE-cadherin, ZO-1, Occludin and Cx43 expressions in retina ($n=6$). **i-k** MDA, NADPH and GSH concentrations in retinal sections ($n=6$). ##$p<0.01$ vs. the control, *$p<0.05$, **$p<0.01$ vs. DR group or the indicated group

hyperlipidemia, and hypertension, whereas irregular dietary management and metabolic memory phenomenon attenuate the clinical benefit for patients [1]. The effectiveness of simple metabolic control is limited when the mechanism underlying the metabolic disorders-related vascular pathology of DR remains unclear. This study investigates the potential therapeutic effects of Rd on vascular early injury in a mouse model of DR and high glucose-induced RVECs. Mechanistically, Rd specifically enhances AMPK-induced FAO by agonizing GPR30, and the metabolic reprogramming regulated by Rd effectively reverses the increased endothelial permeability and BRB breakdown. The findings not only bolster the robust theoretical foundation for advancing innovative therapeutic avenues targeting DR, but also pave the way for future clinical investigations.

The common pathogenesis in blinding retinal diseases is retinal vascular leakage resulting from the loss of BRB integrity [34]. To maintain physiological homeostasis in the retinal microenvironment, BRB selectively regulates material exchange between the retina and systemic circulation by intercellular physical barrier formed by ECs and other cells involved in BRB [35]. Prior to the manifestation of clinical indications of DR, long-term hyperglycemia could alter the junctional stability resulting in vascular leakage. At this time, pre-clinical diabetic retinopathy (PCDR) is characterized by mild and diffuse BRB injury. As PCDR progresses to NPDR, leaky plasma constituents accumulate in the retina and subsequently form hard exudates. The localized profuse leakage is accompanied by microvascular abnormalities and local tissue ischaemia, which induces an increase in VEGF and further exacerbates barrier instability, promoting neovascularization in PDR. The progressive elevation of endothelial permeability ultimately leads to diabetic macular edema and endangers the vision in the absence of prompt intervention [23, 36]. While the barrier structural and functional disruption is paramount in the initial stages of DR, the precise molecular events in BRB collapse are poorly understood, and various, often conflicting, viewpoints exist. Consequently, there has been little advancement in the approaches to vascular barrier repair, despite the clinical trials of small molecules like CaD, aspirin, and antihistamines [37]. Recent research has shown that the functional roles of individual ginsenosides in vascular remodeling may even be contradictory, depending on their chemical structures and distinct pathophysiological environments [38]. In the present study, Rd is firstly identified as a novel endothelial barrier remediation, effectively alleviating the acute BRB breakdown in a VEGF-induced mouse model and the chronic vascular leakage in a STZ-induced DR model. In vitro experiments further reveal that Rd rectifies vasopermeability of RVECs in response to high glucose through the reconstruction of adhering, tight and gap junctions.

For the complex metabolic diseases, deciphering the deep causes of vascular damage should start with multiple intertwined metabolic disorder. There are systemic and local dysregulation of lipid metabolism in almost all diabetic microvascular complications [39]. In the 1950s, the identification of lipid compositions in hard exudates opened the prelude to clinical and basic research on lipid metabolism in DR [10]. A range of cross-sectional and longitudinal studies have consistently shown an association between the development and progression of DR and traditional serum lipid profiles [10]. Cardiovascular-system-focused clinical trials also investigate the potential benefit of numerous lipid-lowering medications in safeguarding against DR [9–10]. Fenofibrate improves retinal pathology by exerting anti-inflammatory and anti-apoptotic effects on ECs, pericytes and retinal pigment epithelial cells [9, 40]. Lipid metabolic disorder that favors retinal neurovascular injury is a prominent hallmark of DR. But, little efforts have been made to explore potential targetable nodes responsible for the lipid metabolic adaptation of retina under pathological stressors. Our observations reveal for the first time that FAO is a essential metabolic process required for maintenance of the endothelial barrier function in retina. Concurrently, the retinal vasoprotective activity of Rd is at least partially contingent upon revitalization for FAO. The findings align with several notable observations that yield comparable outcomes. Besides that diabetic heart exhibits a decreased mitochondrial β-oxidation, deficient FAO induces renal dysfunction in diabetic nephropathy [41–42]. Acute CPT1A inhibition disrupts vascular integrity by promoting calcium influx [43]. FAO sustains the hexosamine biosynthesis pathway to support protein glycosylation, and then relieves the defects in airway epithelial barrier integrity [44]. Therefore, FAO emerges as a novel druggable checkpoint in governing retinal endothelial permeability. Further understanding of the metabolic plasticity in DR contributes to the advancement of pharmacological strategies capable of covering complex pathological mechanisms and avoiding compensatory regulation.

Although much is known about the role of metabolism in endothelial function, there remains a substantial gap in our knowledge on how metabolic adaptation compromises BRB under hyperglycemic circumstances. Multiple pathways are implicated in the metabolism-driven alterations of cellular function. Firstly, the coupling metabolic network controls biomass flux and metabolic flow. The Warburg effect supports uncontrolled proliferation of cancer cells, and FAO is crucial for *de novo* nucleotide synthesis in ECs [25]. Secondly, certain metabolic intermediates have the ability to function as signaling

molecules. Lactate, an inevitable byproduct of glycolysis, activates GPR81. Additionally, succinate, a TCA cycle organic acid, serves as the natural ligand for GPR91 [45–46]. Third, metabolic intermediates participate in post-translational modification. The ketolysis strengthens the TCA cycle-dependent Ac-CoA production and subsequently histone acetylation, thereby reinforcing $CD8^+$ T cell effector responses [47]. Lastly, metabolic enzymes execute nonmetabolic functions. In cancer, PKM2, glycolytic enzymes, can phosphorylate STAT3 and interact with HIF-1α to promote target genes transcription [48]. Our data indicates that the activated AMPK accelerates FAO and fuel the TCA cycle with Ac-CoA. On the basis of the increased flux in TCA cycle, AMPK facilitates FOXO1-dependent IDH2 expression, and revitalizes the enzymatic activity of IDH2 by the PGC-1α/SIRT3 pathway. This collaborative action sustains NADPH regeneration, effectively reversing the damage caused by mitochondrial ROS on retinal endothelial barriers.

Although NADPH does not exhibit permeability across various cellular compartments, recent evidence has indicated intercommunication between the mitochondrial and cytoplasmic NADPH pools. In ECs treated with TGF-β, excessive glycolysis diminishes cytoplasmic NADPH production, and triggers a compensatory efflux of mitochondrial NADPH through isocitrate/α-ketoglutarate shuttle [49]. Our results cannot exclude the involvement of NADPH crosstalk between the cytosol and mitochondria in DR, and this aspect deserves clarification in following investigation by isotopic metabolic labeling technique.

Excess FAO aggravates myocardial oxidative stress, and the inhibition of FAO has evolved into a recognized approach to treat heart failure associated with diabetes and obesity [50]. This paradoxical phenomenon of FAO in redox regulatory systems may be attributed to distinct cellular energy metabolic preferences. ECs predominantly utilize glycolysis (80–96%) to generate ATP, whereas the healthy adult heart primarily relies on FAO (60–90%) for energy supply [51–52]. Since only a small fraction of glucose (approximately 0.04%) enters the TCA cycle, FAO is the primary source of mitochondrial respiration in ECs [8]. Consequently, it is postulated that mitochondrial oxidative phosphorylation largely assumes a non-metabolic role in endothelial function. More comprehensive exploration is warranted to ascertain the mechanisms underlying the discrepancy of FAO in redox homeostasis management across different cell types.

AMPK, a crucial hub of energy sensing and metabolic control, is a well-received target for ginsenosides. Our previous study also shows that AMPK activation can be achieved by Rd in HUVECs, whereas the upstream of AMPK remains to be elucidated [21]. Only recently has it been demonstrated that Rd phosphorylates AMPK by binding to TAK1 in 3T3-L1 adipocytes [53]. In RVECs, Rd directly stimulates GPR30 and initiates the downstream PKA-LKB1-AMPK nongenomic cascade. However, this is not the sole pathway, as evidenced by the slower increase in phosphorylated AMPK observed in HEK293 cells (no GPR30 expression) incubated with Rd. GPR30, stimulated by β-estradiol, can be classified as a non-classical steroid receptor (G protein-coupled estrogen receptor, GPER). A plethora of steroid hormones have been exhibited to activate AMPK in intact cells [54–55]. The ginsenosides, comprising a cholesterol-like lipophilic steroid skeleton with a range of hydrophilic sugar moieties, have the possibility to interact with multiple steroid receptors [56]. The abundant pharmacological properties of ginsenosides are attributed to their structural similarity to steroid hormones [57]. Notably, the targeting of GPR30 by dammarane-type tetracyclic triterpenoid saponins, including ginsenosides, has not been previously reported. We identify Rd as a novel natural agonist of GPR30, but there is conspicuous room for further progress in determining the structure-activity relationship of ginsenosides and the significance of other steroid receptors in retinal vasoprotective activity. Alternatively, cryoelectron microscopy and 3D reconstruction should be considered for identifying precise interaction sites and bonding patterns between GPR30 and Rd in the future.

In conjunction with the supporting effects of GPR30-selective modulators and GPR30 knockdown approaches, GPR30 is widely involved in the pathogenesis of diseases as diverse as cardiovascular diseases, obesity, diabetes, and cancer [16]. GPR30 knockout mice recapitulate many features of metabolic syndrome related to the disturbances in glucose-lipid metabolism. Simultaneously, GPR30 agonist G1 mitigates obesity and glucose homeostasis resulting from estrogen deficiency and a high fat diet, through the augmentation of energy expenditure and remodeling of adipose tissue [17]. Thus far, the primary focus of researchers has been on the efficacy of GPR30-specific ligands against metabolic syndrome. Our study represents the initial unveiling of the metabolic regulation of GPR30 in nonmetabolic tissue, thereby proposing GPR30 as a promising druggable target for metabolic derangements and their associated complications.

However, numerous significant matters remain to be addressed before researchers can target GPR30 by Rd for DR treatment. While the GPR30-AMPK pathway is a central focus in our current study, the combined research of multiple omics should be applied to unearth the endothelial global impact caused by Rd, and the crosstalk between fatty acid metabolism and additional signaling pathways. The composition of retinal cell types is not monolithic but heterogeneous. Numerous fundamental and clinical evidences show that the degeneration of

retinal ganglion cell precede clinically detectable microvascular impairs in the early DR [58]. In the study, Rd could effectively ameliorate retinal ganglion cell loss and nerve fibre layer thinning in response to hyperglycemia. Based on our previous discovery, ginsenoside Rg1, a structural analogue of Rd, promotes axonal generation of retinal ganglion cells under normal physiological states [59]. We could not completely exclude the potential involvement of neurons, glial cells, and other vascular cells in Rd-mediated therapeutic intervention in DR. Therefore, the ability to comprehensively characterize regulatory of Rd at single-cell level is clearly worth of further investigation. Moreover, our previous study and unpublished data show that ginsenosides exhibit favorable ocular metabolic characteristics when administered topically, which adds further to its pharmaceutical appeal [60]. The systematic research on Rd, such as bioavailability, systemic toxicity and scalability for indications, will ultimately allow clinical translation of these present findings.

In summary, these findings provide valuable insights into the widespread perturbations across a network of metabolic pathways and signaling pathways for BRB homeostasis and function. Hyperglycemia compromises FAO through AMPK inhibition and disrupts mitochondrial redox homeostasis via IDH2-induced NADPH regeneration, which underlies the metabolism behind endothelial barrier dysfunction. Furthermore, the facilitation of AMPK-driven FAO by Rd or other GPR30 agonists targeting this metabolic vulnerability could represent a feasible therapeutic strategy for DR.

Supplementary Information

The online version contains supplementary material available at https://doi.org/10.1186/s12933-025-02638-3.

Supplementary Material 1

Acknowledgements
The graphical abstract was conducted by Figdraw.

Author contributions
NHT, ZW and KT conceived and designed the experiments. KT performed the majority of experiments, analyzed data, and drafted the manuscript. CCH and ZJH performed partial experiments. NHT and ZW supervised the experiments and gave the final approval of the manuscript. NHT refined the manuscript and provided funding. All authors have read and approved the article.

Funding
This work was supported by two grants of National Natural Science Foundation of China (No.32070356 and No.82474065).

Data availability
No datasets were generated or analysed during the current study.

Declarations

Ethics approval and consent to participate
No human patients were included in the study. All animal experiments were performed in accordance with the Guide for Care and Use of Laboratory Animals published by the US National Institutes of Health (NIH publication No. 85 – 23, revised 1996) and approved by the Institutional Animal Care and Use Committee of China Pharmaceutical University and the Institutional Ethics Committee of China Pharmaceutical University (approval number: 2023-08-017).

Consent for publication
All authors have read the paper and agree that it can be published.

Competing interests
The authors declare no competing interests.

Author details
[1]State Key Laboratory of Natural Medicines, Department of TCMs Pharmaceuticals, School of Traditional Chinese Pharmacy, China Pharmaceutical University, 639 Longmian Road, Nanjing 211198, China

Received: 20 November 2024 / Accepted: 7 February 2025
Published online: 14 March 2025

References

1. Cheung N, Mitchell P, Wong T. Diabetic retinopathy. Lancet. 2010;376(9735):124–36. https://doi.org/10.1016/S0140-6736(09)62124-3.
2. Antonetti DA, Klein R, Gardner TW. Diabetic retinopathy. N Engl J Med. 2012;366(13):1227–39. https://doi.org/10.1056/NEJMra1005073
3. Hou X, Wang L, Zhu D, et al. Prevalence of diabetic retinopathy and vision-threatening diabetic retinopathy in adults with diabetes in China. Nat Commun. 2023;14(1):4296. https://doi.org/10.1038/s41467-023-39864-w.
4. Levine SR, Sapieha P, Dutta S, et al. It is time for a moonshot to find cures for diabetic retinal disease. Prog Retin Eye Res. 2022;90:101051. https://doi.org/10.1016/j.preteyeres.2022.101051.
5. Stitt AW, Curtis TM, Chen M, et al. The progress in understanding and treatment of diabetic retinopathy. Prog Retin Eye Res. 2016;51:156–86. https://doi.org/10.1016/j.preteyeres.2015.08.001.
6. Wong TY, Cheung CM, Larsen M, et al. Diabetic retinopathy. Nat Rev Dis Primers. 2016;2:16012. https://doi.org/10.1038/nrdp.2016.12.
7. Li X, Sun X, Carmeliet P. Hallmarks of endothelial cell metabolism in health and disease. Cell Metab. 2019;30(3):414–33. https://doi.org/10.1016/j.cmet.2019.08.011.
8. Eelen G, de Zeeuw P, Treps L, et al. Endothelial cell metabolism. Physiol Rev. 2018;98(1):3–58. https://doi.org/10.1152/physrev.00001.2017.
9. Busik JV. Lipid metabolism dysregulation in diabetic retinopathy. J Lipid Res. 2021; 62: 100017. https://doi.org/10.1194/jlr.TR120000981
10. Jenkins AJ, Grant MB, Busik JV. Lipids, hyperreflective crystalline deposits and diabetic retinopathy: potential systemic and retinal-specific effect of lipid-lowering therapies. Diabetologia. 2022;65(4):587–603. https://doi.org/10.1007/s00125-022-05655-z
11. Schoors S, de Bock K, Cantelmo AR, et al. Partial and transient reduction of glycolysis by PFKFB3 blockade reduces pathological angiogenesis. Cell Metab. 2014;19(1):37–48. https://doi.org/10.1016/j.cmet.2013.11.008.
12. Zhang J, Wu Y, Zhang J, et al. ABCA1 deficiency-mediated glomerular cholesterol accumulation exacerbates glomerular endothelial injury and dysfunction in diabetic kidney disease. Metabolism. 2023;139:155377. https://doi.org/10.1016/j.metabol.2022.155377.
13. Herzig S, Shaw RJ. AMPK: guardian of metabolism and mitochondrial homeostasis. Nat Rev Mol Cell Biol. 2018;19(2):121–35. https://doi.org/10.1038/nrm.2017.95.
14. Shrikanth CB, Nandini CD. AMPK in microvascular complications of diabetes and the beneficial effects of AMPK activators from plants. Phytomedicine. 2020;73:152808. https://doi.org/10.1016/j.phymed.2018.12.031.
15. Sekar P, Hsiao G, Hsu SH, et al. Metformin inhibits methylglyoxal-induced retinal pigment epithelial cell death and retinopathy via AMPK-dependent mechanisms: reversing mitochondrial dysfunction and upregulating glyoxalase 1. Redox Biol. 2023;64:102786. https://doi.org/10.1016/j.redox.2023.102786.

16. Prossnitz ER, Barton M. The G protein-coupled oestrogen receptor GPER in health and disease: an update. Nat Rev Endocrinol. 2023;19(7):407–24. https://doi.org/10.1038/s41574-023-00822-7.
17. Sharma SG, Hu C, Staquicini DI, et al. Preclinical efficacy of the GPER-selective agonist G-1 in mouse models of obesity and diabetes. Sci Transl Med. 2020;12(528):5956. https://doi.org/10.1126/scitranslmed.aau5956
18. Zhu GX, Zuo JL, Xu L, et al. Ginsenosides in vascular remodeling: cellular and molecular mechanisms of their therapeutic action. Pharmacol Res. 2021;169:105647. https://doi.org/10.1016/j.phrs.2021.105647.
19. Zhu G, Zuo J, Xu L, et al. Systematic evaluation of combined herbal adjuvant therapy for proliferative diabetic retinopathy. Front Endocrinol. 2023;14:1157189. https://doi.org/10.3389/fendo.2023.1157189.
20. Chen Y, Liu Q, An P, et al. Ginsenoside Rd: a promising natural neuroprotective agent. Phytomedicine. 2022;95:153883. https://doi.org/10.1016/j.phymed.2021.153883.
21. Tang K, Qin W, Wei R, et al. Ginsenoside Rd ameliorates high glucose-induced retinal endothelial injury through AMPK-STRT1 interdependence. Pharmacol Res. 2022;179:106123. https://doi.org/10.1016/j.phrs.2022.106123.
22. Wang Y, Sun X, Xie Y, et al. *Panax notoginseng* saponins alleviate diabetic retinopathy by inhibiting retinal inflammation: association with the NF-κB signaling pathway. J Ethnopharmacol. 2024;319(Pt1):117135. https://doi.org/10.1016/j.jep.2023.117135.
23. Klaassen I, Van Noorden CJ, Schlingemann RO. Molecular basis of the inner blood-retinal barrier and its breakdown in diabetic macular edema and other pathological conditions. Prog Retin Eye Res. 2013;34:19–48. https://doi.org/10.1016/j.preteyeres.2013.02.001
24. Kalucka J, Bierhansl L, Conchinha NV, et al. Quiescent endothelial cells upregulate fatty acid β-oxidation for vasculoprotection via redox homeostasis. Cell Metab. 2018;28(6):881–94. https://doi.org/10.1016/j.cmet.2018.07.016.
25. Schoors S, Bruning U, Missiaen R, et al. Fatty acid carbon is essential for dNTP synthesis in endothelial cells. Nature. 2015;520(7546):192–7. https://doi.org/10.1038/nature14362.
26. Prossnitz ER, Arterburn JB. International union of basic and clinical pharmacology. XCVII. G protein-coupled estrogen receptor and its pharmacologic modulators. Pharmacol Rev. 2015;67(3):505–40. https://doi.org/10.1124/pr.114.009712.
27. Hao F, Tian M, Zhang X, et al. Butyrate enhances CPT1A activity to promote fatty acid oxidation and iTreg differentiation. Proc Natl Acad Sci U S A. 2021;118(22):e2014681118. https://doi.org/10.1073/pnas.2014681118.
28. Wang R, Lou X, Feng G, et al. IL-17A-stimulated endothelial fatty acid β-oxidation promotes tumor angiogenesis. Life Sci. 2019;229:46–56. https://doi.org/10.1016/j.lfs.2019.05.030.
29. Peoples JN, Saraf A, Ghazal N, et al. Mitochondrial dysfunction and oxidative stress in heart disease. Exp Mol Med. 2019;51(12):1–13. https://doi.org/10.1038/s12276-019-0355-7.
30. Shao C, Lu W, Du Y, et al. Cytosolic ME1 integrated with mitochondrial IDH2 supports tumor growth and metastasis. Redox Biol. 2020;36:101685. https://doi.org/10.1016/j.redox.2020.101685.
31. Zhou X, Chen M, Zeng X, et al. Resveratrol regulates mitochondrial reactive oxygen species homeostasis through Sirt3 signaling pathway in human vascular endothelial cells. Cell Death Dis. 2014;5(12):e1576. https://doi.org/10.1038/cddis.2014.530.
32. Li Y, Liu Y, Liu S, et al. Diabetic vascular diseases: molecular mechanisms and therapeutic strategies. Signal Transduct Target Ther. 2023;8(1):152. https://doi.org/10.1038/s41392-023-01400-z.
33. Iruela-Arispe ML. How to target vascular leakage in retinopathy: could a lipid tighten the pipes. EMBO Mol Med. 2023;15(5):e17520. https://doi.org/10.15252/emmm.202317520.
34. Antonetti DA, Silva PS, Stitt AW. Current understanding of the molecular and cellular pathology of diabetic retinopathy. Nat Rev Endocrinol. 2021;17(4):195–206. https://doi.org/10.1038/s41574-020-00451-4.
35. Rudraraju M, Narayanan SP, Somanath PR. Regulation of blood-retinal barrier cell-junctions in diabetic retinopathy. Pharmacol Res. 2020;161:105115. https://doi.org/10.1016/j.phrs.2020.105115.
36. Roy S, Jiang JX, Li A, Kim D. Connexin channel and its role in diabetic retinopathy. Prog Retin Eye Res. 2017;61:35–59. https://doi.org/10.1016/j.preteyeres.2017.06.001.
37. Kim K, Maharjan S, Lim C, et al. Glucal-conjugated sterols as novel vascular leakage blocker: structure-activity relationship focusing on the C17-side chain. Eur J Med Chem. 2014;75:184–94. https://doi.org/10.1016/j.ejmech.2014.01.027.
38. Sarhene M, Ni J, Duncan ES, et al. Ginsenosides for cardiovascular diseases; update on pre-clinical and clinical evidence, pharmacological effects and the mechanisms of action. Pharmacol Res. 2021;166:105481. https://doi.org/10.1016/j.phrs.2021.105481.
39. Eid S, Sas KM, Abcouwer SF, et al. New insights into the mechanisms of diabetic complications: role of lipids and lipid metabolism. Diabetologia. 2019;62(9):1539–49. https://doi.org/10.1007/s00125-019-4959-1.
40. Shao Y, Chen J, Dong L, et al. A protective effect of PPARα in endothelial progenitor cells through regulating metabolism. Diabetes. 2019;68(11):2131–42. https://doi.org/10.2337/db18-1278.
41. Qin X, Jiang M, Zhao Y, et al. Berberine protects against diabetic kidney disease via promoting PGC-1α-regulated mitochondrial energy homeostasis. Br J Pharmacol. 2020;177(16):3646–61. https://doi.org/10.1111/bph.14935.
42. Ljubkovic M, Gressette M, Bulat C, et al. Disturbed fatty acid oxidation, endoplasmic reticulum stress, and apoptosis in left ventricle of patients with type 2 diabetes. Diabetes. 2019;68(10):1924–33. https://doi.org/10.2337/db19-0423.
43. Patella F, Schug ZT, Persi E, et al. Proteomics-based metabolic modeling reveals that fatty acid oxidation controls endothelial cell permeability. Mol Cell Proteom. 2015;14(3):621–34. https://doi.org/10.1074/mcp.M114.045575.
44. Crotta S, Villa M, Major J, et al. Repair of airway epithelia requires metabolic rewiring towards fatty acid oxidation. Nat Commun. 2023;14(1):721. https://doi.org/10.1038/s41467-023-36352-z.
45. Feng L, Shang R, Wang X, et al. The natural alkaloid (-)-N-hydroxyapiosporamide suppresses colorectal tumor progression as an NF-κB pathway inhibitor by targeting the TAK1-TRAF6 complex. J Nat Prod. 2023;86(6):1449–62. https://doi.org/10.1021/acs.jnatprod.3c00125.
46. Haffke M, Fehlmann D, Rummel G, et al. Structural basis of species-selective antagonist binding to the succinate receptor. Nature. 2019;574(7779):581–5. https://doi.org/10.1038/s41586-019-1663-8.
47. Luda KM, Longo J, Kitchen-Goosen SM, et al. Ketolysis drives $CD8^+$ T cell effector function through effects on histone acetylation. Immunity. 2023;56(9):2021–35. https://doi.org/10.1016/j.immuni.2023.07.002.
48. Xu D, Shao F, Bian X, et al. The evolving landscape of noncanonical functions of metabolic enzymes in cancer and other pathologies. Cell Metab. 2021;33(1):33–50. https://doi.org/10.1016/j.cmet.2020.12.015.
49. Zeng H, Pan T, Zhan M, et al. Suppression of PFKFB3-driven glycolysis restrains endothelial-to-mesenchymal transition and fibrotic response. Signal Transduct Target Ther. 2022;7(1):303. https://doi.org/10.1038/s41392-022-01097-6.
50. Abdurrachim D, Luiken JJ, Nicolay K, et al. Good and bad consequences of altered fatty acid metabolism in heart failure: evidence from mouse models. Cardiovasc Res. 2015;106(2):194–205. https://doi.org/10.1093/cvr/cvv105.
51. Hurley JB, Lindsay KJ, Du J. Glucose, lactate, and shuttling of metabolites in vertebrate retinas. J Neurosci Res. 2015;93(7):1079–92. https://doi.org/10.1002/jnr.23583.
52. Lopaschuk GD, Karwi QG, Tian R, et al. Cardiac energy metabolism in heart failure. Circ Res. 2021;128(10):1487–513. https://doi.org/10.1161/CIRCRESAHA.121.318241.
53. Wan S, Cui Z, Wu L, et al. Ginsenoside Rd promotes omentin secretion in adipose through TBK1-AMPK to improve mitochondrial biogenesis via WNT5A/Ca^{2+} pathways in heart failure. Redox Biol. 2023;60:102610. https://doi.org/10.1016/j.redox.2023.102610.
54. Li S, Song Z, Yan Y, et al. Aldosterone from endometrial glands is benefit for human decidualization. Cell Death Dis. 2020;11(8):679. https://doi.org/10.1038/s41419-020-02844-9.
55. Zucchetti AE, Barosso IR, Boaglio AC, et al. G-protein-coupled receptor 30/adenylyl cyclase/protein kinase A pathway is involved in estradiol 17β-D-glucuronide-induced cholestasis. Hepatology. 2014;59(3):1016–29. https://doi.org/10.1002/hep.26752.
56. Park J, Song H, Kim SK, et al. Effects of ginseng on two main sex steroid hormone receptors: estrogen and androgen receptors. J Ginseng Res. 2017;41(2):215–21. https://doi.org/10.1016/j.jgr.2016.08.005.
57. Park J, Bui PTC, Song H, et al. Ginseng on nuclear hormone receptors. Am J Chin Med. 2017;45(6):1147–56. https://doi.org/10.1142/S0192415X17500628.
58. Sun W, An X, Zhang Y, et al. The ideal treatment timing for diabetic retinopathy: the molecular pathological mechanisms underlying early-stage diabetic retinopathy are a matter of concern. Front Endocrinol. 2023;14:1270145. https://doi.org/10.3389/fendo.2023.1270145.
59. Jiang Y, Wei R, Tang K, et al. Ginsenoside Rg1 promotes neurite growth of retinal ganglion cells through cAMP/PKA/CREB pathways. J Ginseng Res. 2024;48(2):163–70. https://doi.org/10.1016/j.jgr.2022.05.002.

60. Wei R, Jiang Y, Tang K, et al. Simultaneous determination of *Panax notoginseng* total saponins in rabbit tears by UPLC-QqQ-MS/MS and its application to pharmacokinetic study. J Chromatogr B Analyt Technol Biomed Life Sci. 2023;1218:123490. https://doi.org/10.1016/j.jchromb.2022.123490.

Publisher's note